Inorganic Chemistry

Article

pubs.acs.org/IC

Effects of Heteroatoms on Electronic States of Divanadium-Substituted γ-Keggin-type Polyoxometalates

Kazuhiro Uehara,[†] Takuya Miyachi,[†] Takahito Nakajima,[‡] and Noritaka Mizuno*[,†]

[†]Department of Applied Chemistry, School of Engineering, The University of Tokyo, 7-3-1 Hongo, Bunkyo-ku, Tokyo 113-8656, Japan

[‡]RIKEN Advanced Institute for Computational Science, Computational Molecular Science Research Team, 7-1-26, Minatojima-minami-machi, Chuo-ku, Kobe, Hyogo, 650-0047, Japan

Supporting Information

ABSTRACT: Effects of heteroatoms on electronic states of divanadium-substituted γ-Keggin-type polyoxometalates $(TBA)_4[\gamma\text{-}XV_2W_{10}O_{38}(\mu\text{-}OH)(\mu\text{-}OR)]$ (X = Ge, Si; R = Me, Et, *n*-Pr, H; TBA = tetra(*n*-butyl)ammonium) and $(TBA)_4[\gamma\text{-}XV_2W_{10}O_{38}(\mu\text{-}O)]$ (X = Ge, Si) were investigated, using a combination of nuclear magnetic resonance spectroscopy and density functional theory (DFT) calculations. Both the substitution of SiO_4 heteroatom units with larger GeO_4 ones and the introduction of more electronegative alkoxo groups in place of hydroxo groups resulted in deshielding of the vanadium nuclei. DFT calculations using the Def2-SVP basis set at TPSSh level of theory could well-reproduce the anionic moieties of a series of divanadium-substituted γ-Keggin-type polyoxometalates, and the estimated chemical shifts approximately reproduced the experimental ones with the individual gauge localized orbital method (SO-IGLO) taking the spin−orbit interaction into account. The magnetic shielding (σ) consists of $\sigma_d + \sigma_p + \sigma_{SD} + \sigma_{FC}$, where σ_d, σ_p, σ_{SD}, and σ_{FC} are diamagnetic, paramagnetic, spin-dipolar, and Fermi contact terms, respectively. The σ_p changed much among $(TBA)_4[\gamma\text{-}XV_2W_{10}O_{38}(\mu\text{-}OH)_2]$, $(TBA)_4[\gamma\text{-}XV_2W_{10}O_{38}(\mu\text{-}OH)(\mu\text{-}OR)]$, and $(TBA)_4[\gamma\text{-}XV_2W_{10}O_{38}(\mu\text{-}O)]$, while σ_d, σ_{SD}, and σ_{FC} did not change much. Therefore, the σ_p largely contributed to the magnetic shielding. Moreover, σ_p consisted of the occupied−occupied transitions (s-terms) and the occupied−virtual ones (u-terms), and the u-terms were predominant for σ_p. The most contributing occupied localized orbital consisted of the d_z^2 orbital of vanadium, the p_z orbital of terminal oxygen related to the V═O bond, and the p_z orbital of oxygen of the XO_4 unit, whereas the two virtual localized orbitals consisted of the d_{yz} orbital of vanadium and the p_y orbital of terminal oxygen. Analysis of the structural and electronic characteristics of a series of divanadium-substituted γ-Keggin-type POMs revealed a linear correlation between both $^{51}V\{H\}$ chemical shifts and the reciprocal values of the energy gaps between the corresponding XO_4-predominant orbital HOMOs-X and the LUMOs+X (X = 0, 1, or 2). All these results indicate that neighboring XO_4 units weakly interact with the addenda atoms and control the electronic states of polyoxometalates and the magnetic shielding of their addenda atoms.

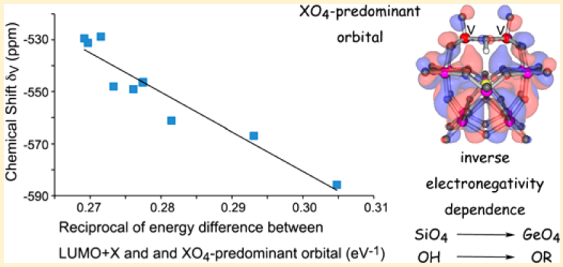

INTRODUCTION

Vanadium is one of the essential elements and is frequently found in the active centers of several enzymes, including haloperoxidase and nitrogenase, as well as insulin mimetic compounds.[1] For this reason, numerous oxo and peroxo vanadium complexes that mimic the active centers of such compounds have been widely studied to date.[2] Since the ^{51}V nucleus has a nuclear spin of 7/2 and its natural abundance is 99.75%, nuclear magnetic resonance (NMR) spectroscopy is a powerful tool for elucidating the environment in the vicinity of active vanadium centers.[1−3] In general, the magnetic shielding of main group elements increases as the number of the electron-donating ligands (or substituents) increases or as the electronegativity of the ligand decreases. The effects of halogen substituents on the magnetic shielding of the nucleus have been studied, which corresponds to the latter scenario, and it has been found that the magnetic shielding increases in the order of F < Cl < Br < I, which is the so-called normal electronegativity dependence.[4] In contrast, some high-valent early transition metals, such as Ti, Mo, and V, do not follow this trend and instead result in inverse electronegativity dependence.[5] Experimental and theoretical studies have shown that the nature of the direct chemical bond between the substituent and the observed nucleus contributes to the dependence, and this factor may be expressed as the paramagnetic contribution of the shielding constant (σ_p) in Ramsey's equation.[1a,6] Although much effort has been applied to investigating correlations between the electronic states and magnetic shielding of small compounds, such as mono- or dinuclear complexes, our understanding of the multinuclear complexes, such as polyoxometalates (POMs), is still incomplete.[7−10]

POMs are anionic metal oxide clusters consisting primarily of early transition metals and oxo moieties, and have been utilized

Received: March 6, 2014
Published: March 28, 2014

   dx.doi.org/10.1021/ic5005209 | *Inorg. Chem.* 2014, 53, 3907−3918

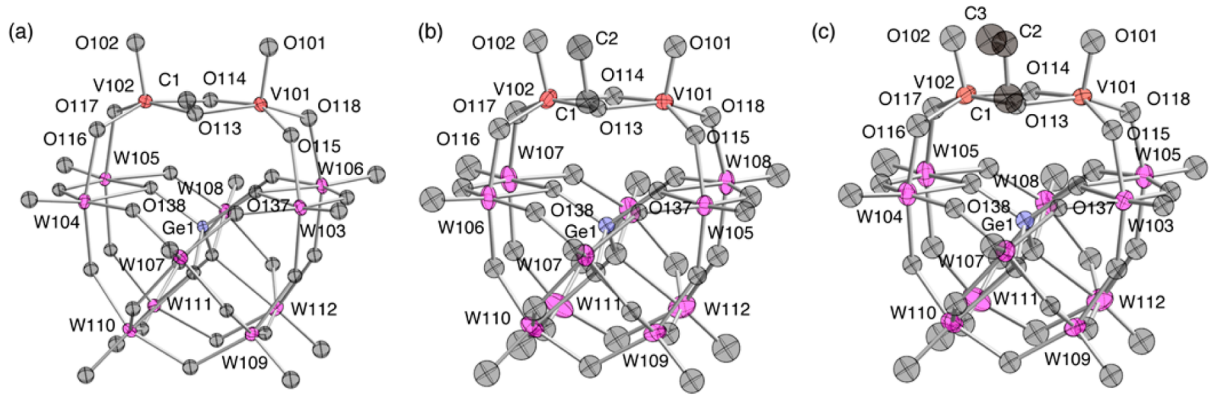

Figure 1. Thermal ellipsoid plots of $(TBA)_4[\gamma\text{-}GeV_2W_{10}O_{38}(\mu\text{-}OH)(\mu\text{-}OR)]$ $\mathbf{2^X{\cdot}R}$ (R = (a) Me, (b) Et, (c) Pr) at the 50% probability level (TBA was omitted for clarity).

Table 1. Crystallographic Data for $(TBA)_4[\gamma\text{-}XV_2W_{10}O_{38}(\mu\text{-}OH)(\mu\text{-}OR)]$ $2^X{\cdot}R$ (X = Ge, Si; R = Me, Et, Pr)

compound	$\mathbf{2^{Ge}{\cdot}Me}$	$\mathbf{2^{Ge}{\cdot}Et}$	$\mathbf{2^{Ge}{\cdot}Pr}$	$\mathbf{2^{Si}{\cdot}Me}$	$\mathbf{2^{Si}{\cdot}Et}$	$\mathbf{2^{Si}{\cdot}Pr}$
empirical formula	$C_{65}GeN_4O_{40}V_2W_{10}$	$C_{66}GeN_4O_{40}V_2W_{10}$	$C_{67}GeN_4O_{40}V_2W_{10}$	$C_{65}N_4O_{40}SiV_2W_{10}$	$C_{66}GeN_4O_{40}V_2W_{10}$	$C_{67}GeN_4O_{40}V_2W_{10}$
formula weight	3489.66	3501.67	3513.68	3445.16	3457.17	3469.18
crystal system	monoclinic	orthorhombic	orthorhombic	orthorhombic	monoclinic	orthorhombic
lattice type	primitive	primitive	primitive	primitive	primitive	primitive
space group	$P2_1$ (No. 4)	$Pna2_1$ (No. 33)	$Pna2_1$ (No. 33)	$P2_12_12_1$ (No. 19)	$Pna2_1$ (No. 33)	$Pna2_1$ (No. 33)
lattice parameter	a = 18.23170(10) Å	a = 24.5651(2) Å	a = 24.5272(110) Å	a = 24.0164(3) Å	a = 24.5529(2) Å	a = 24.6549(2) Å
	b = 14.48250(10) Å	b = 25.1254(3) Å	b = 25.0227(13) Å	b = 30.9323(5) Å	b = 25.1124(2) Å	b = 25.1382(2) Å
	c = 18.6286(10) Å	c = 17.2009(2) Å	c = 17.3856(9) Å	c = 14.7456(2) Å	c = 17.16510(10) Å	c = 17.20050(10) Å
	β = 94.5(0)°					
	V = 4903.56(7) Å^3	V = 10616.5(2) Å^3	V = 10670.2(9) Å^3	V = 10954.2(3) Å^3	V = 10583.70(5) Å^3	V = 10660.52(14) Å^3
Z	2	4	4	4	4	4
d_{calcd}	2.363 g cm^{-3}	2.191 g cm^{-3}	2.187 g cm^{-3}	2.089 g cm^{-3}	2.17 g cm^{-3}	2.162 g cm^{-3}
F_{000}	3112	6248	6272	6152	6176	6200
μ (Mo Kα)	12.232 mm^{-1}	11.3 mm^{-1}	11.244 mm^{-1}	10.693 mm^{-1}	11.068 mm^{-1}	10.989 mm^{-1}
no. of reflections measured	13828	15062	14745	16125	15174	14484
no. of observations	13315	13855	12752	12404	14439	13840
no. of variables	505	314	315	314	313	320
$R_1{}^a$	0.0388	0.0712	0.0819	0.0813	0.0737	0.0486
$wR_2{}^a$	0.126	0.1773	0.1876	0.2053	0.1559	0.1323

[a]Data with $I > 2.00\sigma(I)$.

as catalysts, pharmaceuticals, magnetic materials, and inorganic−organic hybrid materials.[11,12] When POMs are employed as catalysts, the design and fabrication of the active sites within the cluster are important, as is an understanding of the electronic states. Although it has been noted that the particular heteroatom units (XO_4) in POMs can be used to adjust their anionic charges and that HOMO−LUMO energy gaps likely affect the reactivity of these complexes, there are few experimental results concerning the functions of the XO_4 units.[13,14] In addition, little is known about substituent effects on the electronic states of POMs, due to difficulty in introducing different substituents into the POM framework.[15]

Recently, (μ-oxo)divanadium-substituted γ-Keggin-type POMs such as $(TBA)_4[\gamma\text{-}XV_2W_{10}O_{38}(\mu\text{-}O)]$ $\mathbf{3^X}$ (X = Ge, Si; TBA = tetra(*n*-butyl)ammonium) have been synthesized, and the ^{51}V MAS NMR chemical shifts of the four-coordinated vanadium nuclei have been observed at higher magnetic fields (X = Ge, −566.90 ppm; Si, −585.80 ppm) compared to the shifts seen for the six- and five-coordinated bis(μ-hydroxo)-divanadium-substituted γ-Keggin-type POMs $(TBA)_4[\gamma\text{-}XV_2W_{10}O_{38}(\mu\text{-}OH)_2]$ $\mathbf{1^X}$ (X = Ge, −546.28 ppm; Si, −561.20 ppm).[16] These remarkably increased magnetic field shifts prompted us to investigate the reason for the phenomena. In this article, a series of organic-soluble alkoxo derivatives of the divanadium-substituted γ-Keggin-type POMs $(TBA)_4[\gamma\text{-}XV_2W_{10}O_{38}(\mu\text{-}OH)(\mu\text{-}OR)]$ $\mathbf{2^X{\cdot}R}$ (X = Ge, Si; R = Me, Et, Pr) are synthesized, and the effects of XO_4 units on the electronic states of the addenda atoms in divanadium(V)-substituted γ-Keggin-type POMs ($\mathbf{1^X}$, $\mathbf{2^X{\cdot}R}$, and $\mathbf{3^X}$) are investigated by a combination of multinuclear NMR spectroscopy and density functional theory (DFT) calculations with the individual gauge localized orbital method (SO-IGLO) taking the spin−orbit interaction into account.

dx.doi.org/10.1021/ic5005209 | *Inorg. Chem.* 2014, 53, 3907−3918

Table 2. Selected Bond Distances and Angles for $(TBA)_4[\gamma\text{-}XV_2W_{10}O_{38}(\mu\text{-}OH)(\mu\text{-}OR)]$ $2^X\cdot R$ (X = Ge, Si; R = Me, Et, Pr)

complex	$2^{Ge}\cdot Me$	$2^{Ge}\cdot Et$	$2^{Ge}\cdot Pr$	$2^{Si}\cdot Me$	$2^{Si}\cdot Et$	$2^{Si}\cdot Pr$
V═O	1.583(12), 1.608(12)	1.55(2), 1.59(2)	1.55(2), 1.57(3)	1.66(3), 1.64(3)	1.58(2), 1.59(2)	1.625(14), 1.604(16)
V−O(−V)	1.967(10), 1.988(10)	1.954(15), 1.998(17)	1.99(2), 2.014(19)	1.96(2), 1.957(19)	1.978(16), 1.958(17)	1.987(13), 1.948(12)
	1.958(11), 1.971(10)	1.945(15), 1.962(17)	1.976(19), 1.948(19)	1.90(2), 1.928(18)	1.976(16), 1.941(17)	1.992(12), 1.941(12)
V−O(−W)	1.822(11), 1.827(11)	1.852(17), 1.87(2)	1.821(19), 1.85(2)	1.84(2), 1.89(2)	1,808(17), 1.825(18)	1.838(12), 1.855(12)
	1.833(10), 1.841(10)	1.85(2), 1.803(18)	1.79(2), 1.86(2)	1.90(3), 1.85(2)	1.807(17), 1.789(17)	1.795(12), 1.829(11)
V···O(−X)	2.392(9), 2.362(9)	2.451(16), 2.431(19)	2.444(18), 2.415(19)	2.58(2), 2.60(3)	2.56(2), 2.53(2)	2.58(1), 2.53(1)
X−O	1.749(8), 1.752(9)	1.705(16), 1.740(14)	1.733(18), 1.753(18)	1.643(19), 1.61(2)	1.622(15), 1.668(15)	1.616(10), 1.640(11)
	1.707(10), 1.757(8)	1.748(16), 1.733(19)	1.714(19), 1.82(2)	1.624(19), 1.615(18)	1.616(16), 1.606(18)	1.651(10), 1.647(12)
X···V	3.729(5), 3.720(7)	3.761(9), 3.748(5)	3.76(1), 3.742(6)	3.805(8), 3.811(8)	3.821(9), 3.804(7)	3.788(7), 3.782(4)
V···V	3.156(4)	3.169(9)	3.17(1)	3.118(8)	3.137(9)	3.118(3)
O···O	5.31(2), 5.32(2)	5.34(3), 5.31(3)	5.30(4), 5.35(3)	5.36(4), 5.30(4)	5.21(3), 5.22(3)	5.22(2), 5.24(2)
(lacunary site)	2.73(2), 2.73(2)	2.70(3), 2.75(3)	2.72(3), 2.64(3)	2.68(3), 2.75(4)	2.66(3), 2.70(3)	2.69(2), 2.72(2)
V−O−V	107.0(5), 105.7(5)	108.8(7), 106.3(8)	106.1(9), 106.3(9)	107.7(10), 106.8(9)	105.0(7), 107.1(8)	103.1(6), 106.6(6)
torsion angle[a]	0.098	3.081	2.659	0.182	3.184	0.790

[a] O(101)−V(101)···V(102)−O(102) angle.

RESULTS AND DISCUSSION

Syntheses of $(TBA)_4[\gamma\text{-}XV_2W_{10}O_{38}(\mu\text{-}OH)(\mu\text{-}OR)]$ $2^X\cdot R$ (X = Ge, Si; R = Me, Et, Pr). Initially, organic-soluble TBA salts of alkoxo derivatives of the divanadium-substituted γ-Keggin-type POMs $(TBA)_4[\gamma\text{-}XV_2W_{10}O_{38}(\mu\text{-}OH)(\mu\text{-}OR)]$ $2^X\cdot R$ (X = Ge, Si; R = Me, Et, Pr) were synthesized by reactions of $(TBA)_4[\gamma\text{-}XV_2W_{10}O_{38}(\mu\text{-}OH)_2]$ 1^X with excess amounts of the appropriate alcohol (ROH, R = Me, Et, Pr) in acetonitrile ($2^{Ge}\cdot Me$, 67% yield; $2^{Ge}\cdot Et$, 83%; $2^{Ge}\cdot Pr$ 92%; $2^{Si}\cdot Me$, 55%; $2^{Si}\cdot Et$, 76%; $2^{Si}\cdot Pr$, 61%).[17] All compounds were characterized by infrared spectroscopy (IR), NMR spectroscopy, cold-spray ionization mass spectrometry (CSI-MS), elemental analysis, and X-ray crystallography (Figures 1 and S1−S6 Supporting Information and Tables 1 and 2).

During the synthetic procedure, one of the two hydroxo groups in 1^X reacts with the alcohol to introduce an alkoxo group between the vanadium centers. The bond valence sum (BVS) values of V (4.82−5.10), W (5.86−6.80), Ge or Si (3.95−4.19), and O (1.55−2.30) for $2^X\cdot R$ indicate that the respective valences of these atoms are 5, 6, 4, and −2 (Tables S1−S6, Supporting Information).[18] The BVS values of the O(114) bridging oxygen atoms in the $2^X\cdot R$ series were 1.21−1.42, suggesting that the hydroxide ligands are maintained. The Ge−O distances (1.707(10)−1.82(2) Å) in $2^{Ge}\cdot R$ were significantly longer than those in $2^{Si}\cdot R$ (1.61(2)−1.668(15) Å) since the covalent radius of Ge (1.22 Å) is greater than that of Si (1.11 Å). Accordingly, the vacant site sizes in $2^{Ge}\cdot R$ (5.30(4)−5.35(3) Å; 2.64(3)−2.75(3) Å) were slightly larger than those in $2^{Si}\cdot R$ (5.21(3)−5.36(4) Å; 2.66(3)−2.75(4) Å). The V···V distances in $2^{Ge}\cdot R$ (3.156(4)−3.17(1) Å) were longer than those in $2^{Si}\cdot R$ (3.118(3)−3.137(9) Å), whereas the V···O(−Ge) distances in $2^{Ge}\cdot R$ (2.362(9)−2.451(16) Å) were shorter than the V···O(−Si) distances in $2^{Si}\cdot R$ (2.53(1)−2.60(3) Å). These results reveal the expansion and deposition of the $(\mu\text{-}OR)(\mu\text{-}OH)V_2$ core upon the substitution of Si^{4+} with Ge^{4+}.

The reactions of 1^X with alcohols produced only mono alkoxo derivatives ($2^X\cdot R$) despite the use of excess amounts of alcohol. Calculated values of $pK_a(1)$ = 16.42 and $pK_a(2)$ = 21.52 for 1^{Ge} and values of $pK_a(1)$ = 15.12 and $pK_a(2)$ = 22.19 for 1^{Si} have recently been reported.[16a] One of the two hydroxides in 1^X therefore acts as a base in reactions with alcohols, since the pK_a values for methanol, ethanol, and *n*-propanol are 15.5, 15.9, and 16.2, respectively, all of which are significantly lower than the $pK_a(2)$ values for 1^X. The pK_a values for deprotonation from $2^{Ge}\cdot R$ to $[\gamma\text{-}GeV_2W_{10}O_{38}(\mu\text{-}OR)(\mu\text{-}O)]^{5-}$ are 18.30, 17.43, and 17.99, respectively, whereas those for deprotonation from $2^{Si}\cdot R$ to $[\gamma\text{-}SiV_2W_{10}O_{38}(\mu\text{-}OR)(\mu\text{-}O)]^{5-}$ are 17.91, 17.7, and 17.25 (Table 3). The

Table 3. Calculated pK_a Values of $(TBA)_4[\gamma\text{-}XV_2W_{10}O_{38}(\mu\text{-}OH)(\mu\text{-}OR)]$ (X = Ge, Si); R = Me, Et, Pr)[a]

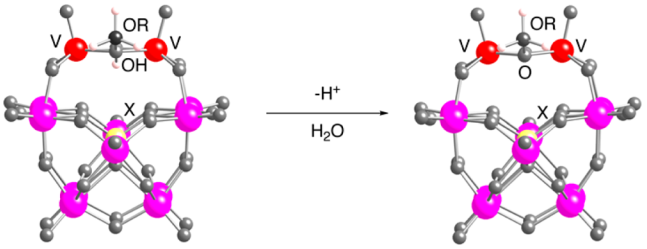

X	R	$V_2(\mu\text{-}OR)(\mu\text{-}OH)$[b]	$V_2(\mu\text{-}O)(\mu\text{-}OR)$[b]	$\Delta G°$	pK_a[d]
Ge	Me	−5949.80139364	−5949.33789076	104.40	18.30
	Et	−5989.12939429	−5988.66779368	98.43	17.43
	Pr	−6028.45652379	−6027.99368318	102.66	17.99
Si	Me	−4164.30883943	−4163.84617426	102.20	17.91
	Et	−4203.63902567	−4203.17733187	99.65	17.47
	Pr	−4242.96368130	−4242.50245403	98.43	17.25

[a] $\Delta G^{solv}(H_3O^+)$ = −265.9 kcal mol^{-1}. [b] Energy in hartree. [c] Energy in kJ mol^{-1}. [d] $pK_a = (\log_{10}e)(\Delta G°/RT)$.

second dehydrative condensation reaction between $2^X\cdot R$ and an alcohol does not proceed to any appreciable extent likely because the pK_a values for $2^X\cdot R$ are close to those of the alcohols.

DFT Calculations of $[\gamma\text{-}XV_2W_{10}O_{38}(\mu\text{-}OH)(\mu\text{-}OR)]^{4-}$. To obtain additional insights into the electronic structures of the anionic moieties of the alkoxo derivatives $2^X\cdot R$ and the effects of introducing more electronegative alkoxo ligands into the POM frameworks, DFT calculations were carried out in acetonitrile (ε = 35.688) using a conductor-like polarizable continuum model at TPSSh/Def2-SVP level of theory (Figures 2−4 and Table 4).[19−23] The optimized structures were more accurate than those optimized with 6-31G*/LanL2DZ hybrid basis set at B3LYP level of theory in our previous reports.[16] The HOMO energies for $2^{Si}\cdot Me$, $2^{Si}\cdot Et$, and $2^{Si}\cdot Pr$ were −6.932, −6.914, and −6.919 eV, respectively, and LUMO

dx.doi.org/10.1021/ic5005209 | Inorg. Chem. 2014, 53, 3907−3918

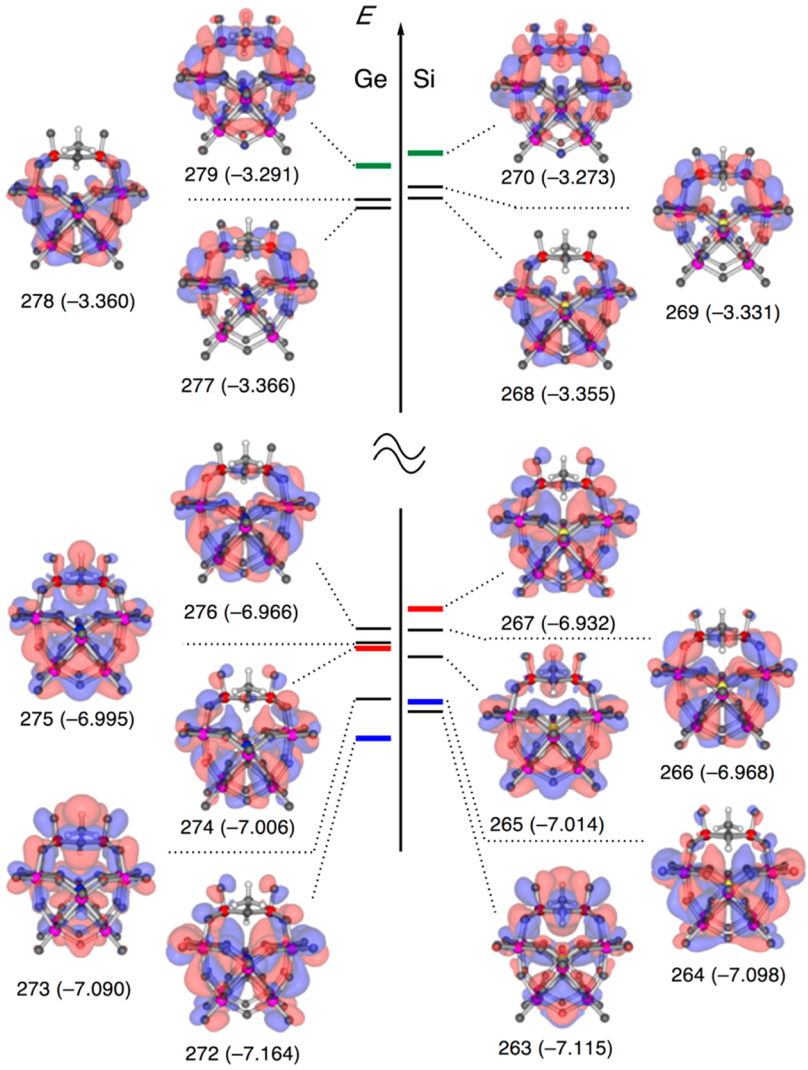

Figure 2. Selected molecular orbitals of $(TBA)_4[\gamma\text{-}XV_2W_{10}O_{38}(\mu\text{-}OH)(\mu\text{-}OMe)]$ $\mathbf{2^{X}\cdot Me}$ (X = Ge, Si). Isosurface value: 0.010; energies in parentheses are in eV; blue: positive phase, red: negative phase. The red and blue lines represent the energy levels of XO_4-predominant orbitals, and the green lines represent the energy levels of the most probable virtual orbitals for the transition.

energies for $\mathbf{2^{Si}\cdot Me}$, $\mathbf{2^{Si}\cdot Et}$, and $\mathbf{2^{Si}\cdot Pr}$ were −3.355 eV, −3.371 eV, and −3.365 eV. Thus, the HOMO and LUMO energies and HOMO−LUMO energy gaps ($\Delta E'$; 3.543 − 3.577 eV) of $\mathbf{2^{Si}\cdot R}$ were almost close to one another and independent of R. The LUMO energies for $\mathbf{2^{Ge}\cdot Me}$, $\mathbf{2^{Ge}\cdot Et}$, and $\mathbf{2^{Ge}\cdot Pr}$ were −3.366 eV, −3.378 eV, and −3.375 eV, respectively, and almost close to one another, and the HOMO energy for $\mathbf{2^{Ge}\cdot Pr}$ (−6.863 eV) was higher than those of $\mathbf{2^{Ge}\cdot Me}$ (−6.966 eV) and $\mathbf{2^{Ge}\cdot Et}$ (−6.970 eV). As a result, the HOMO−LUMO energy gap for $\mathbf{2^{Ge}\cdot Pr}$ (3.518 eV) was smaller than those of $\mathbf{2^{Ge}\cdot Me}$ (3.592 eV) and $\mathbf{2^{Ge}\cdot Et}$ (3.600 eV).

The HOMOs of $\mathbf{2^{Si}\cdot R}$ predominantly represented the p_z orbitals of O137 and O138 of SiO_4 unit (SiO_4-predominant orbital), and the respective orbital coefficients were 0.21138, 0.22588, and 0.20880. On the other hand, the corresponding GeO_4-predominant orbitals of $\mathbf{2^{Ge}\cdot R}$ were HOMOs-2, and their energies were −7.006 eV (Me), −7.010 eV (Et), and −7.004 (Pr), respectively. The orbital coefficients of GeO_4-predominant orbitals were in the range of 0.10506 − 0.12319 and smaller than those of $\mathbf{2^{Si}\cdot R}$, because the deeper depositions of the $(OV)_2(\mu\text{-}OH)(\mu\text{-}OR)$ cores into the $[\gamma\text{-}GeW_{10}O_{36}]^{8-}$ frameworks stabilized HOMOs-2 of $\mathbf{2^{Ge}\cdot R}$ in comparison with HOMOs of $\mathbf{2^{Si}\cdot R}$. The weaker interactions between the divanadium cores and SiO_4-predominant orbitals were also confirmed by the smaller orbital coefficients of d_{z^2} orbital of vanadium of $\mathbf{2^{Si}\cdot R}$ (0.00093−0.00373) than those of $\mathbf{2^{Ge}\cdot R}$ (0.01273−0.01454).

In addition, HOMOs-2 of $\mathbf{2^{Si}\cdot Me}$ (−7.014 eV) and $\mathbf{2^{Si}\cdot Et}$ (−7.002 eV) and HOMO-1 of $\mathbf{2^{Si}\cdot Pr}$ (−6.921 eV) represented the V−OR bonds, and their stabilities decreased in the order of $\mathbf{2^{Si}\cdot Me}$ > $\mathbf{2^{Si}\cdot Et}$ > $\mathbf{2^{Si}\cdot Pr}$. The corresponding orbitals of $\mathbf{2^{Ge}\cdot R}$ were HOMOs-1 of $\mathbf{2^{Ge}\cdot Me}$ (−6.995 eV) and $\mathbf{2^{Ge}\cdot Et}$ (−6.974 eV) and HOMO of $\mathbf{2^{Ge}\cdot Pr}$ (−6.863 eV), and their stabilities decreased in the same order of $\mathbf{2^{Ge}\cdot Me}$ > $\mathbf{2^{Ge}\cdot Et}$ > $\mathbf{2^{Ge}\cdot Pr}$. These orders are the same as that of nucleophilicities of alkoxides (MeO > EtO > PrO). These orbital energies of $\mathbf{2^{Ge}\cdot R}$ were larger than those of $\mathbf{2^{Si}\cdot R}$, likely because of the stronger electronic repulsion between the R-O orbital and the p_z orbitals of O137 and O138 by deeper depositions of the $(OV)_2(\mu\text{-}OH)(\mu\text{-}OR)$ cores into the $[\gamma\text{-}GeW_{10}O_{36}]^{8-}$ frameworks. Therefore, the weakest nucleophilicity of propoxide and the stronger electronic repulsions of $\mathbf{2^{Ge}\cdot R}$ between the R-O orbitals and the p_z orbitals of O137 and O138 than those of $\mathbf{2^{Si}\cdot}$

dx.doi.org/10.1021/ic5005209 | Inorg. Chem. 2014, 53, 3907−3918

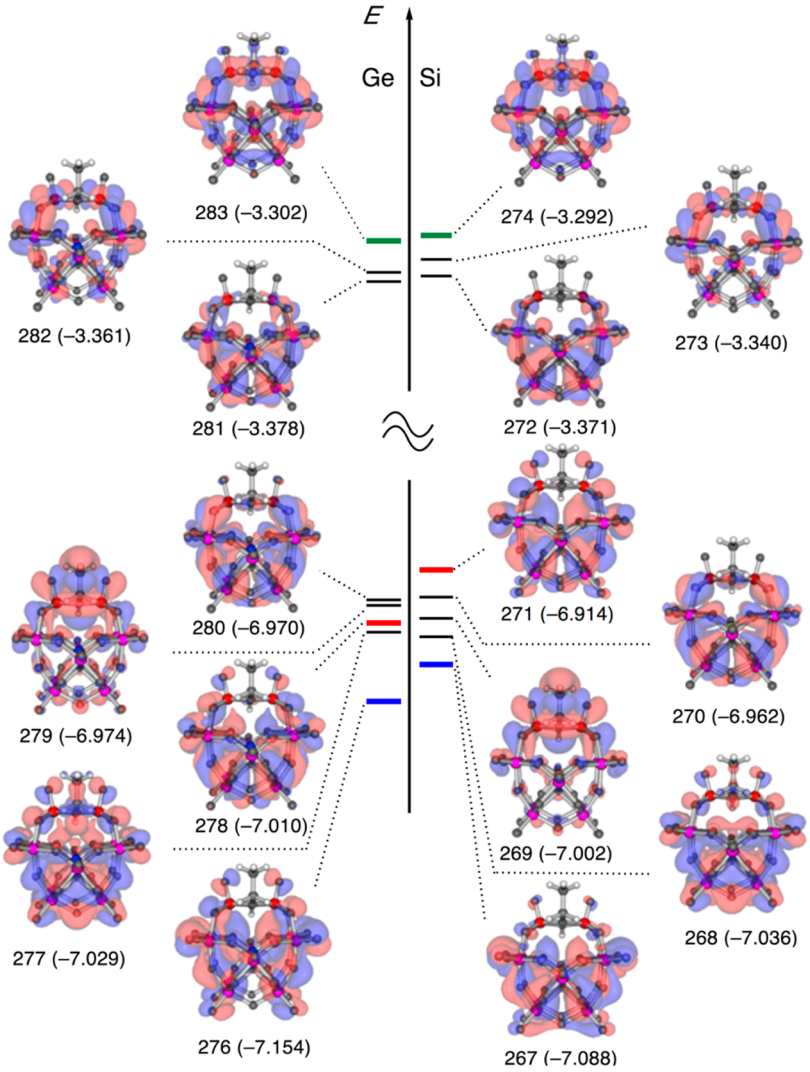

Figure 3. Selected molecular orbitals of $(TBA)_4[\gamma\text{-}XV_2W_{10}O_{38}(\mu\text{-}OH)(\mu\text{-}OEt)]$ $\mathbf{2^X}$**·Et** (X = Ge, Si). Isosurface value: 0.010; energies in parentheses are in eV; blue: positive phase, red: negative phase. The red and blue lines represent the energy levels of XO_4-predominant orbitals and the green lines represent the energy levels of the most probable virtual orbitals for the transition.

R would result in the highest energy level of HOMO of $\mathbf{2^{Ge}}$**·Pr** as described above.

Effects of Heteroatom Units on the Electronic States of Substituted Vanadium Atoms in POMs. The NMR spectroscopy becomes a powerful method to elucidate the electronic states of the transition metal complexes. The approximate Ramsey's equation for the paramagnetic term achieves a great success to explain the substituent effects, such as normal and inverse electronegativity dependences, with the linear relationships between the chemical shifts and the reciprocal values of HOMO−LUMO energy gaps. Hill et al. have reported that the heteroatom (X) in $[(X^{n+}O_4)Ru_2(OH)_2(M_{FW})_{10}O_{32}]^{(8-n)-}$ (M_{FM} = Mo and W, and X = Al^{III}, Si^{IV}, P^V, and S^{VI}) can function as "internal switches" capable of controlling the ground electronic states.[13b] It has been recognized that the XO_4 orbitals of α- or β-Keggin-type POMs frequently become HOMOs.[14a] However, no correlations between chemical shifts and electronic states have been elucidated for different kinds of POMs.[7−10,13,14] This is likely because NMR measurements have been frequently performed in $H(D)_2O$, where chemical shifts are dependent on the pH of the solution,[24] and the approximate Ramsey's equation for the paramagnetic term might not be applicable to the larger complex systems. Therefore, to evaluate the electronic environments of the addenda atoms in POMs, (i) the magnetic shielding of a series of organic-soluble TBA salts of divanadium substituted POMs: $(TBA)_4[\gamma\text{-}XV_2W_{10}O_{38}(\mu\text{-}OH)_2]$ $\mathbf{1^X}$, $(TBA)_4[\gamma\text{-}XV_2W_{10}O_{38}(\mu\text{-}OH)(\mu\text{-}OR)]$ $\mathbf{2^X}$**·R**, and $(TBA)_4[\gamma\text{-}XV_2W_{10}O_{38}(\mu\text{-}O)]$ $\mathbf{3^X}$ was investigated experimentally and (ii) the details of magnetic shielding in a series of POMs were examined with DFT calculations.

(a). $^{51}V\{H\}$ NMR. The $^{51}V\{H\}$ NMR signals of $\mathbf{2^{Ge}}$**·Me**, $\mathbf{2^{Ge}}$**·Et**, $\mathbf{2^{Ge}}$**·Pr**, $\mathbf{2^{Si}}$**·Me**, $\mathbf{2^{Si}}$**·Et**, and $\mathbf{2^{Si}}$**·Pr** in CD_3CN were observed at −529.44, −531.17, −528.78, −548.09, −549.09, and −546.55 ppm, respectively (Table 4 and Figures S13, S15−S17, S19, and S20, Supporting Information). These chemical shifts show only minimal change with variations in the alkoxo ligands. The $^{51}V\{H\}$ NMR signals of $\mathbf{1^{Ge}}$ and $\mathbf{1^{Si}}$ were observed at −546.28 and −561.20 ppm, respectively. Upon the substitution of the more electronegative methoxo ligand for a hydroxo group in $\mathbf{1^X}$, downfield shifts by 15.11−17.5 ppm on going from $\mathbf{1^{Ge}}$ to $\mathbf{2^{Ge}}$**·R** and by 12.11−14.65 ppm on going from $\mathbf{1^{Si}}$ to $\mathbf{2^{Si}}$**·R** were observed, which demonstrates the expected electronegativity dependence. Conversely, upon

dx.doi.org/10.1021/ic5005209 | Inorg. Chem. 2014, 53, 3907−3918

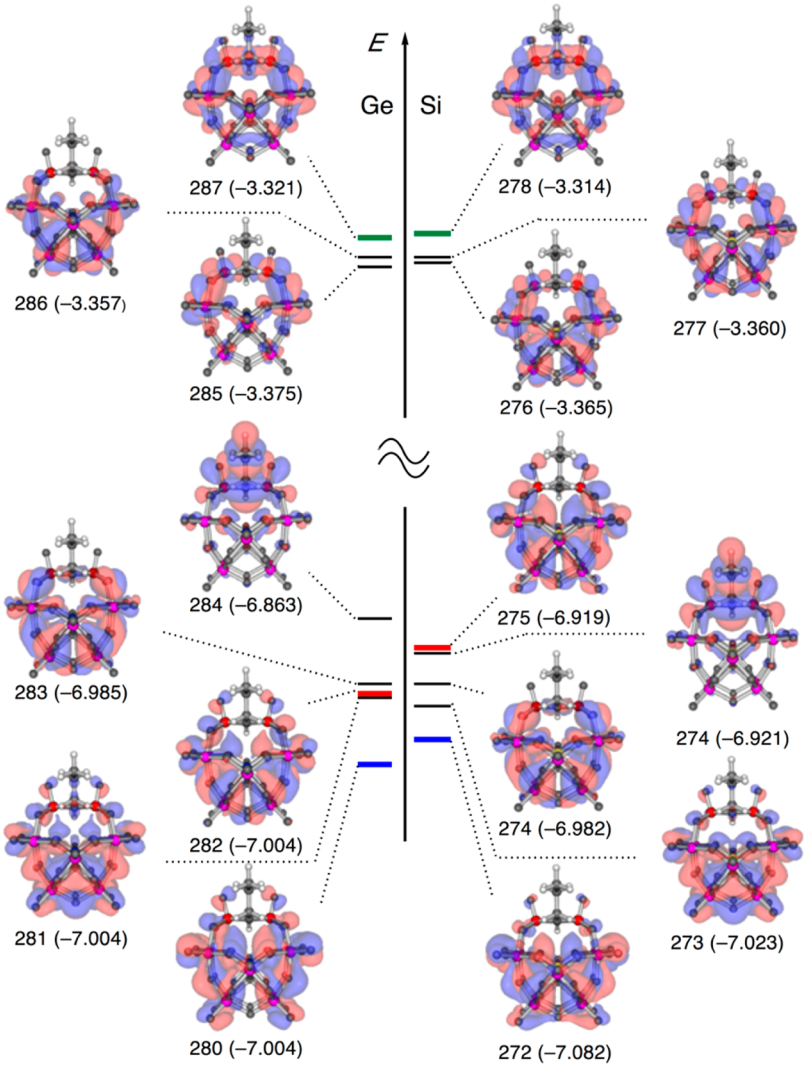

Figure 4. Selected molecular orbitals of $(TBA)_4[\gamma\text{-}XV_2W_{10}O_{38}(\mu\text{-}OH)(\mu\text{-}OPr)]$ $\mathbf{2^X{\cdot}Pr}$ (X = Ge, Si). Isosurface value: 0.010; energies in parentheses are in eV; blue: positive phase, red: negative phase. The red and blue lines represent the energy levels of XO_4-predominant orbitals, and the green lines represent the most probable virtual orbitals for the transition.

Table 4. Selected Features of the Divanadium-Substituted γ-Keggin-type Polyoxometalates $(TBA)_4[\gamma\text{-}XV_2W_{10}O_{38}(\mu\text{-}OH)(\mu\text{-}OR)]$ (X = Ge, Si; R = Me, Et, Pr, 2X·R; R = H, 1^X) and $(TBA)_4[\gamma\text{-}XV_2W_{10}O_{38}(\mu\text{-}O)]$ 3^X (X = Ge, Si)

		δ_W (ppm)			V···O(−X)	$\Delta E'$	ΔE	orbital coefficients[i]	
compd	δ_V (ppm)	W103−W106	W107, W108	W109−W112	(Å)[e]	(eV)[f]	(eV)[g]	p_z (O)	d_{z^2} (V)
$\mathbf{2^{Ge}{\cdot}Mee}$	−529.44	−52.34, −63.65	−71.93, −102.90	−98.58, −109.64	2.377	3.600	3.715	0.10506	0.01454
$\mathbf{2^{Ge}{\cdot}Et}$	−531.17	−53.23, −65.71	−75.08, −101.00	−99.19, −107.92	2.441	3.592	3.708	0.12319	0.01273
$\mathbf{2^{Ge}{\cdot}Pr}$	−528.78	−54.44, −66.62	−76.39, −102.48	−100.26, −109.06	2.4295	3.518	3.683	0.12055	0.01344
$\mathbf{2^{Si}{\cdot}Me}$	−548.05	−80.29, −93.97	−93.08, −122.82	−124.07, −134.2	2.590	3.577	3.659	0.21138	0.00373
$\mathbf{2^{Si}{\cdot}Et}$	−549.09	−82.43, −96.23	−95.91, −121.35	−124.83, −132.61	2.545	3.543	3.622	0.22588	0.00284
$\mathbf{2^{Si}{\cdot}Pr}$	−546.55	−81.59, −95.69	−95.69, −121.49	−124.51, −132.31	2.555	3.554	3.605	0.20880	0.00093
$\mathbf{1^{Ge}}$[b]	−546.28[b]	−56.07	−78.76	−105.20	2.4135	3.537	3.604	0.09102	0.00321
$\mathbf{1^{Si}}$[c]	−561.20[c]	−82.74	−96.41	−129.77	2.520	3.553	3.553	0.16646	0.00281
$\mathbf{3^{Ge}}$[a]	−566.90[b,d]	*h*	*h*	*h*	2.5635	3.412	3.412	0.19369	0.00322
$\mathbf{3^{Si}}$[a]	−585.80[c,d]	*h*	*h*	*h*	2.733	3.281	3.281	0.26569	0.00282

[a] $\mathbf{3^X}$ = $(TBA)_4[\gamma\text{-}XV_2W_{10}O_{38}(\mu\text{-}O)]$ (X = Ge, Si). [b] Reported in ref 15a. [c] Reported in ref 15b. [d] Determined by ^{51}V MAS NMR. [e] Averaged distance. [f] HOMO−LUMO energy difference. [g] XO_4-predominant orbital-LUMO+X energy difference (X = 0, 1, or 2). [h] ^{183}W MAS NMR spectra could not be obtained. [i] Absolute values of coefficients for the p_z orbitals of O137 (O138) in the XO_4 unit and the d_{z^2} orbital of vanadium.

substitution of the SiO_4 unit with the larger, less electronegative GeO_4 group, downfield shifts by 17.77−18.65 ppm on going from $\mathbf{2^{Si}{\cdot}R}$ to $\mathbf{2^{Ge}{\cdot}R}$ and by 14.92 ppm on going from $\mathbf{1^{Si}}$ to $\mathbf{1^{Ge}}$ were observed, in the same manner as the 18.90 ppm downfield shift observed on going from $\mathbf{3^{Si}}$ to $\mathbf{3^{Ge}}$, showing an inverse electronegativity dependence. Thus, two different types of

dx.doi.org/10.1021/ic5005209 | Inorg. Chem. 2014, 53, 3907−3918

dependence on magnetic shielding were observed in a series of divanadium-substituted γ-Keggin-type POMs.

(b). Correlation between Chemical Shifts and V···O(−X) Distances. First of all, we focus on the distances around vanadium atoms such as V···V, V−O(−V), V−O(−W), and V═O, and no correlations between these distances and chemical shifts were observed. On the other hand, the distances between vanadium atoms and O(−X) atoms are correlated with ^{51}V chemical shifts (Figure 5), while the O(−X) atoms are

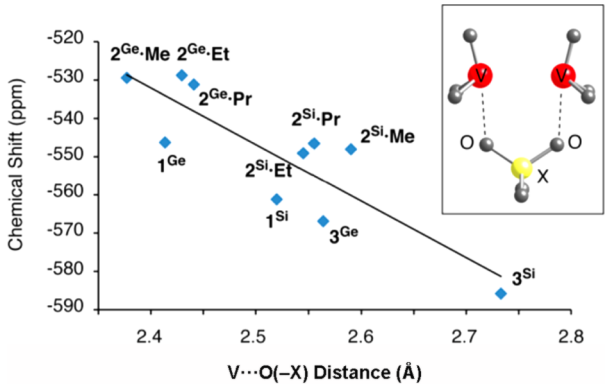

Figure 5. Correlation between chemical shifts (δ_V) and V···O−(X) distances.

positioned out of the coordination sphere of vanadium centers: As the V···O(−X) distances in $\mathbf{1}^{X}$ and $\mathbf{2}^{X}$**·R** with the square pyramidal vanadium centers and $\mathbf{3}^{X}$ with four-coordinated tetrahedral vanadium centers increased, ^{51}V chemical shifts in $\mathbf{1}^{X}$, $\mathbf{2}^{X}$**·R**, and $\mathbf{3}^{X}$ shifted toward higher magnetic field regions. These results suggest that the O(−X) atoms possibly control the electronic state of the vanadium atoms. A similar distant effect of the nitrogen atom at the axial position on the ^{14}N chemical shift has been reported in ref 25b, and these considerations are reasonable from the coordination chemical point of view.

(c). ^{51}V Chemical Shifts of a Series of Divanadium Substituted γ-Keggin type Polyoxometalates Calculated with DFT. There are several reports on the determination of ^{183}W chemical shifts of several iso- or heteropolyoxometalates with the theoretical calculations.[7−10] To the best of our knowledge, adequate results have recently been obtained with the Slater-type all electron basis set (i.e., TZP) taking into account the relativistic effect (zeroth-order regular approximation, ZORA) and the spin orbit (SO) coupling by Bonchio et al.[10a] and Poblet et al.[8b] Poblet et al. have reported that "Only the occupied−virtual transitions, which are determined by the geometry of the anion, are the principal contributions in the variation of the paramagnetic shielding with small corrections in the spin−oribit term". The octahedral structure of the WO_6 moieties and their W−O distances are important factors controlling the ^{183}W chemical shifts, in accordance with the fact that the chemical shifts principally depend on the local geometries (i.e., coordination environments) around the observed nucleus (e.g., W, V, Pt).[26] On the contrary, prior to this report, Kazansky and Poblet have reported that the occupied−occupied transition (s-term) is more important than the occupied−unoccupied transition (u-term) to determine the paramagnetic contribution of the shielding constant of POMs such as $[W_6O_{19}]^{2-}$, $[W_{10}O_{32}]^{4-}$, and $[\alpha-\beta-\gamma\text{-}XW_{12}O_{40}]^{n-}$. Therefore, much room remains to discuss the prerequisite factors in detail to determine the magnetic shielding in large POM systems. Therefore, we attempted (i) to optimize structures of a series of divanadium substituted POMs with the appropriate basis set (i.e., Def2-SVP) at the better DFT functional theory (TPSSh) with Gaussian09 as the initial structures and (ii) to calculate the magnetic shielding of ^{51}V nucleus of those compounds in acetonitrile using Sapporo-DKH3-TZP-2012 (+ diffuse 1s1p without polarized g; V), Sapporo-DKH3-DZP-2012 (Ge, W), and Sapporo-DZP-2012 (H, O, Si)[27] hybrid basis sets with the individual gauge for localized orbital method (SO-IGLO) of NTChem,[28] taking into account the spin-free one-electron third-order Douglas−Kroll Hamiltonian with the first-order screened nuclear spin−orbit Hamiltonian, at the B97D level of theory.[29] The results are provided in Table 5.

The shielding constants (σ) for $\mathbf{2}^{Ge}$**·Me**, $\mathbf{2}^{Ge}$**·Et**, $\mathbf{2}^{Ge}$**·Pr**, $\mathbf{2}^{Si}$**·Me**, $\mathbf{2}^{Si}$**·Et**, $\mathbf{2}^{Si}$**·Pr**, $\mathbf{1}^{Ge}$, $\mathbf{1}^{Si}$, $\mathbf{3}^{Ge}$, and $\mathbf{3}^{Si}$ were estimated to be −1419.61, −1411.70, −1412.01, −1403.40, −1397.47, −1395.16, −1406.95, −1392.31, −1337.55, and −1322.59 ppm, respectively. The respective chemical shifts for $\mathbf{2}^{Ge}$**·Me**, $\mathbf{2}^{Ge}$**·Et**, $\mathbf{2}^{Ge}$**·Pr**, $\mathbf{2}^{Si}$**·Me**, $\mathbf{2}^{Si}$**·Et**, $\mathbf{2}^{Si}$**·Pr**, $\mathbf{1}^{Ge}$, $\mathbf{1}^{Si}$, $\mathbf{3}^{Ge}$, and $\mathbf{3}^{Si}$ were −515.33, −523.25, −522.93, −531.54, −537.47, −539.78, −527.99, −542.64, −597.39, and −612.36 ppm and approximately reproduced the experimental ones. Therefore, the magnetic shielding and the electronic states of a series of

Table 5. Details of Shielding Constants of the Divanadium-Substituted γ-Keggin-type Polyoxometalates $(TBA)_4[\gamma\text{-}XV_2W_{10}O_{38}(\mu\text{-}OH)(\mu\text{-}OR)]$ (X = Ge, Si; R = Me, Et, Pr, 2^{X}·R; R = H, 1^{X}) and $(TBA)_4[\gamma\text{-}XV_2W_{10}O_{38}(\mu\text{-}O)]$ 3^{X} (X = Ge, Si)

	diamagnetic term (σ_d, ppm)	paramagnetic term (σ_p, ppm)	spin-dipolar term (σ_{SD}, ppm)	Fermi contact term (σ_{FC}, ppm)	total (σ, ppm)	chemical shift (δ_V, ppm)[a]
$\mathbf{2}^{Ge}$**·Me**	1766.69	−3176.11	−6.09	−4.12	−1419.62	−515.32
$\mathbf{2}^{Ge}$**·Et**	1754.50	−3164.13	−6.03	−4.42	−1411.70	−523.25
$\mathbf{2}^{Ge}$**·Pr**	1754.50	−3156.04	−6.07	−4.46	−1412.06	−522.88
$\mathbf{2}^{Si}$**·Me**	1765.95	−3158.91	−5.86	−4.58	−1403.40	−531.54
$\mathbf{2}^{Si}$**·Et**	1762.14	−3148.71	−5.78	−5.11	−1397.47	−537.47
$\mathbf{2}^{Si}$**·Pr**	1753.66	−3137.91	−5.83	−5.09	−1395.16	−539.78
$\mathbf{1}^{Ge}$	1772.32	−3169.26	−5.94	−4.07	−1406.95	−527.99
$\mathbf{1}^{Si}$	1771.72	−3153.78	−5.71	−4.53	−1392.31	−542.64
$\mathbf{3}^{Ge}$	1758.04	−3080.71	−5.89	−8.99	−1337.55	−597.39
$\mathbf{3}^{Si}$	1752.30	−3059.10	−5.68	−10.11	−1322.59	−612.36
$VOCl_3$	1761.56	−3690.07	−9.89	3.46	−1934.94	0

[a]The chemical shift is defined by δ_V (ppm) = $\sigma(VOCl_3) - \sigma$.

dx.doi.org/10.1021/ic5005209 | Inorg. Chem. 2014, 53, 3907−3918

Table 6. Details of Paramagnetic Shielding Constants of the Divanadium-Substituted γ-Keggin-type Polyoxometalates $(TBA)_4[\gamma\text{-}XV_2W_{10}O_{38}(\mu\text{-}OH)(\mu\text{-}OR)]$ (X = Ge, Si; R = Me, Et, Pr, 2^X·R; R = H, 1^X) and $(TBA)_4[\gamma\text{-}XV_2W_{10}O_{38}(\mu\text{-}O)]$ 3^X (X = Ge, Si)

	paramagnetic term (ppm)		
	total	occ−occ[a]	occ−vir[a]
2^{Ge}·Me	−3176.11	129.29	−3305.40
2^{Ge}·Et	−3164.13	129.89	−3294.03
2^{Ge}·Pr	−3156.04	130.12	−3286.16
2^{Si}·Me	−3158.91	128.59	−3287.50
2^{Si}·Et	−3148.71	130.31	−3279.02
2^{Si}·Pr	−3137.91	130.15	−3268.06
1^{Ge}	−3169.26	129.27	−3298.53
1^{Si}	−3153.78	128.76	−3282.55
3^{Ge}	−3080.71	135.78	−3216.50
3^{Si}	−3059.10	137.38	−3196.48

[a]The occupied and virtual orbitals are abbreviated as occ and vir, respectively.

divanadium substituted γ-Keggin-type POMs are discussed below in more detail.

$$\sigma = \sum_{i}^{occ} \left\langle \phi_i^{(0)} \middle| \hat{H}_i^{(\mu,B)} \middle| \phi_i^{(0)} \right\rangle - 2 \sum_{i}^{occ} \left\langle \phi_i^{(0)} \middle| \hat{H}^{\wedge}{}_i^{(\mu)} \middle| \phi_i^{(B)} \right\rangle \quad (1)$$

The magnetic shielding (σ) is defined by eq 1, leading to $\sigma = \sigma_d + \sigma_p + \sigma_{SD} + \sigma_{FC}$, where σ_d, σ_p, σ_{SD}, and σ_{FC} are diamagnetic, paramagnetic, spin-dipolar, and Fermi contact terms, respectively, and σ_p primarily contributes to σ in general.[6] In fact, σ_p changed much among 1^X, 2^X·R, and 3^X, while σ_d, σ_{SD}, and σ_{FC} did not change much (Table 5). Consequently, σ_p largely contributed to the magnetic shielding.

Next, we focus on the details of σ_p (Tables 5 and S7), which consists of the occupied−occupied transitions (s-terms) and the occupied−virtual ones (u-terms). The u-terms were predominant for the paramagnetic term of the shielding constant and decreased in the order of 3^{Si} (−3059.10) < 3^{Ge} (−3080.71) < 1^{Si} (−3153.78) < 2^{Si}·R (−3137.91 to −3158.91) < 1^{Ge} (−3169.26) < 2^{Ge}·R (−3156.04 to −3176.11 ppm). The s-terms were almost constant among these compounds (128.59−137.38 ppm). If the complete basis set is employed, the contributions of the s-terms are ideally zero. The appearances of the s-terms are possibly explained by the gauge-dependence in spite of the gauge-independent physical quantity.

It is worth noting that the SO-IGLO method can depict the localized orbitals contributing to the magnetic shielding. In the paramagnetic terms, the larger contributions of the components less than −220 ppm are listed in Table 7, and the corresponding molecular orbitals are depicted in Figure 6. The main component of the paramagnetic shielding for each compounds was derived from the V═O moiety, which contributed to 38.0−40.8% of the paramagnetic shielding of the vanadium nuclei (Table 7). As these solutions become complex numbers because of a variational consideration of the spin-oribit (SO) coupling, the square of orbitals is drawn in Figures 6, S30 and S31 as the corresponding localized orbital. The most contributing occupied localized orbital consisted of the d_z^2 orbital of vanadium, the p_z orbital of terminal oxygen related to the V═O bond, and the p_z orbital of oxygen of the XO_4 unit (Figure 6a). On the other hand, the virtual localized orbitals consisted of (i) the d_{yz} orbital of vanadium and the p_y orbital of terminal oxygen and (ii) the d_{zx} orbital of vanadium and p_x orbital of terminal oxygen (Figure 6b,c). Accordingly, we attempted to find the canonical molecular orbitals including these orbitals around HOMO and LUMO energy levels. In 2^{Ge}·Me, the corresponding occupied orbitals were HOMO-2 (−7.002 eV) and HOMO-4 (−7.164 eV) (Figure 6d,e), and the corresponding virtual orbitals were LUMO+2 (−3.293 eV) and LUMO+4 (−2.650 eV) (Figure 6f,g). In 2^{Ge}·Et and 2^{Ge}·Pr, the corresponding occupied and virtual orbitals were found at the same energy levels as those in 2^{Ge}·Me. On the other hand, in 2^{Si}·Me, the corresponding occupied orbitals were HOMO (−6.392 eV) and HOMO-3 (−7.098 eV), and the corresponding virtual orbitals were LUMO+2 (−3.273 eV) and LUMO+4 (−2.638 eV). In 2^{Si}·Et and 2^{Si}·Pr, the corresponding occupied orbitals were HOMO and HOMO-4. These observations show that (1) the transitions from the occupied orbitals to the virtual orbitals play an important role to determine the paramagnetic shielding of the vanadium nuclei, (2) the most probable transitions in 2^X·R proceed via the minimum energies from the XO_4-predominant orbital to LUMO+2, and (3) the most probable transitions in 1^X proceed from HOMO-1 to LUMO (Figure S28, Supporting Information), whereas the corresponding transitions in 3^X proceed from HOMO to LUMO (Figure S29, Supporting Information). It is noteworthy that these occupied orbitals weakly interact with O(−X) moieties (Figure 6a,d,e).

Since the virtual−occupied part of the coefficient matrix elements corresponding to Ramsey's equation is represented by eq 6 in the Experimental Section and is proportional to the reciprocal of the energy gaps between occupied and virtual orbitals, a plot of $^{51}V\{H\}$ chemical shifts against reciprocal

Table 7. Main Component of Paramagnetic Shielding Constant Contributing less than −220 ppm

comp	V101−O101 (%) (total, ppm)	V101−O101 (ppm)	V101−O115 (ppm)	V101−O118 (ppm)
2^{Ge}·Me	39.7 (−3176.11)	−712.06, −286.39, −262.57	−264.94	−255.55
2^{Ge}·Et	40.2 (−3164.13)	−704.76, −291.77, −275.58	−273.86	−228.89
2^{Ge}·Pr	40.8 (−3156.04)	−658.27, −331.17, −296.81	−250.93	
2^{Si}·Me	39.9 (−3158.91)	−717.10, −284.23, −258.49	−261.97	−253.15
2^{Si}·Et	40.0 (−3148.71)	−690.35, −293.21, −274.88	−277.70	−220.17
2^{Si}·Pr	40.8 (−3137.91)	−650.01, −333.82, −297.52	−251.97	
1^{Ge}	39.4 (−3169.26)	−728.94, −286.09, −232.45	−252.91	−251.69
1^{Si}	39.6 (−3153.78)	−739.21, −283.66, −225.94	−250.78	−249.28
3^{Ge}	38.0 (−3080.71)	−701.74, −236.22, −234.15	−282.81	−278.76
3^{Si}	38.4 (−3059.10)	−696.98, −240.58, −236.43	−274.84	−272.09

dx.doi.org/10.1021/ic5005209 | Inorg. Chem. 2014, 53, 3907−3918

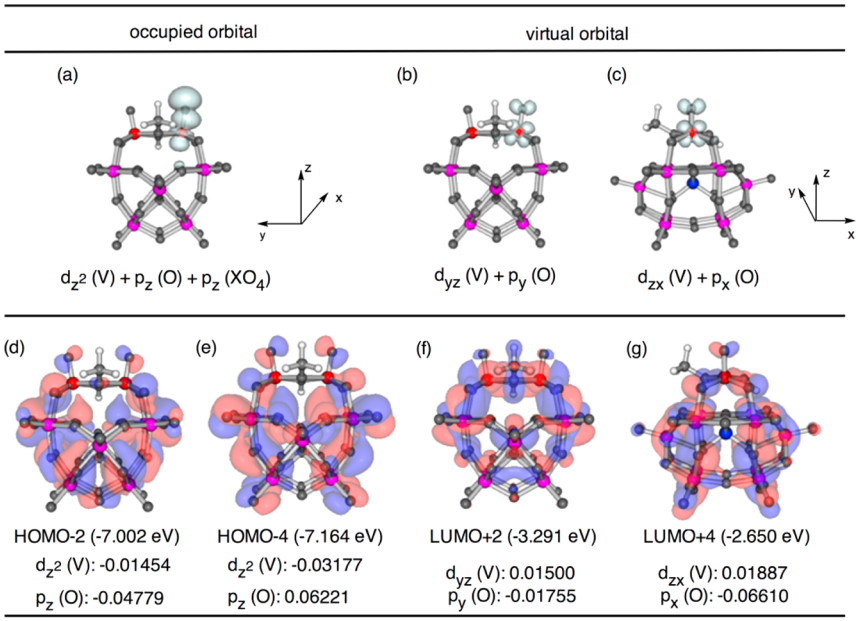

Figure 6. Localized and canonical orbitals mainly contributing to the paramagnetic shielding of vanadium atoms in $\mathbf{2^{Ge}\text{-}Me}$, (a) d_{z^2} (V) + p_z (O) + p_z (XO_4) occupied orbital (isosurface value 0.001), (b) d_{yz} + p_y (O) virtual orbital (isosurface value 0.000002), and (c) d_{zx} (V) + p_x (O) virtual orbital (isosurface value 0.000002), and the corresponding canonical occupied (d and e) and virtual (f and g) orbitals.

values of energy gaps between XO_4-predominalt orbitals and the LUMOs+X (X = 0, 1, or 2; ΔE^{-1}) is provided in Figure 7.

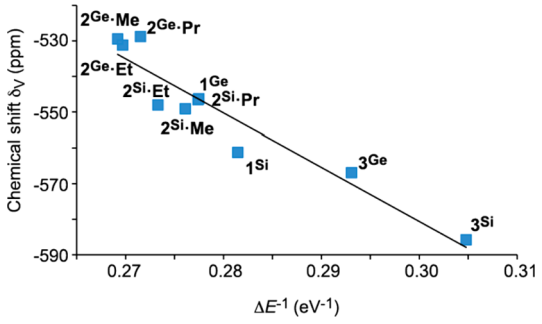

Figure 7. Correlation between chemical shifts (δ_V) and reciprocal values of ΔE.

The chemical shifts linearly decreased with ΔE^{-1}, and a good correlation was observed similarly to Figure 5. It can be seen, therefore, that the XO_4 orbitals have an effect on the electronic states of the addenda atoms of POMs. Taken together, these results lead to the conclusion that neighboring XO_4 units weakly interact with the addenda atoms (V···O(−X)) and control the electronic states of POMs and the magnetic shielding of their addenda atoms.[30]

CONCLUSION

In summary, the effects of substituents and heteroatoms on the divanadium-substituted γ-Keggin-type-POMs $(TBA)_4[\gamma\text{-}XV_2W_{10}O_{38}(\mu\text{-}OH)(\mu\text{-}OR)]$ (X = Ge, Si; R = Me, Et, Pr, H) and $(TBA)_4[\gamma\text{-}XV_2W_{10}O_{38}(\mu\text{-}O)]$ (X = Ge, Si) were investigated using a combination of the NMR spectroscopy and DFT calculations. Following the substitution of SiO_4 units with GeO_4 groups and the introduction of more highly electronegative alkoxo ligands, downfield shifts were observed in the vanadium nuclei, demonstrating an inverse electronegativity dependence. DFT calculations using the Def2-SVP basis set at the TPSSh level of theory could well-reproduce the anionic moieties of a series of divanadium substituted γ-Keggin-type polyoxometalates, and the estimated chemical shifts approximately reproduced the experimental ones with the individual gauge localized orbital method (SO-IGLO) taking the spin−orbit interaction into account. The most contributing occupied localized orbital consisted of the d_{z^2} orbital of vanadium, the p_z orbital of terminal oxygen related to the V═O bond, and the p_z orbital of oxygen of the XO_4 unit, whereas two virtual localized orbitals consisted of the d_{yz} orbital of vanadium and the p_y orbital of terminal oxygen. Analysis of the structural and electronic characteristics of a series of divanadium-substituted γ-Keggin-type POMs revealed a linear correlation between both $^{51}V\{H\}$ chemical shifts and the reciprocal values of the energy gaps between the corresponding XO_4-predominant orbital HOMOs-X and the LUMOs+X (X = 0, 1, or 2). All these results indicate that neighboring XO_4 units weakly interact with the addenda atoms and control the electronic states of POMs and the magnetic shielding of their addenda atoms.

EXPERIMENTAL SECTION

General Procedures. All experimental work was performed under ambient atmospheric air. All solvents, including acetonitrile (acetonitrile-d_3), methanol, ethanol, propanol, *n*-butyl methyl ether ((*n*-Bu)OMe), diethyl ether (Et_2O), and di(*n*-propyl) ether ($(n\text{-}Pr)_2O$), were used as received with no further purification. The compounds $(TBA)_4[\gamma\text{-}XV_2W_{10}O_{38}(\mu\text{-}OH)_2]$ $\mathbf{1^X}$ (X = Ge, Si) were synthesized according to published procedures.[16a,32] ^1H (500 MHz), $^{13}C\{H\}$ (124.50 MHz), $^{29}Si\{H\}$ (98.37 MHz, using DSS (0 ppm) as the standard), $^{51}V\{H\}$ (130.23 MHz, using $NaVO_3$ (−574.28 ppm) as the standard), and ^{183}W NMR (20.81 MHz, using Na_2WO_4 (0 ppm) as the standard) spectra were recorded on JEOL ECA-500. Infrared spectra were obtained using JASCO FT-IR 580. CSI-MS spectra were obtained with JEOL T100-CS. UV−vis spectra were obtained using JASCO V-570. Cyclic voltammgrams were obtained with electrochemical analyzer model 600A (CH Instruments, Inc.).

Syntheses of $(TBA)_4[\gamma\text{-}XV_2W_{10}O_{38}(\mu\text{-}OH)(\mu\text{-}OR)]$ $\mathbf{2^X\text{-}R}$. Compound $\mathbf{1^X}$ (0.050 g, 13.8 μmol for $\mathbf{1^{Ge}}$ and 13.9 μmol for $\mathbf{1^{Si}}$) was dissolved in 2 mL of MeCN along with 1 mL each of MeOH, EtOH,

dx.doi.org/10.1021/ic5005209 | Inorg. Chem. 2014, 53, 3907−3918

and *n*-PrOH, and subsequent layering of (*n*-Bu)OMe, Et_2O, or (*n*-Pr)$_2$O onto the solution gave the corresponding alkoxo derivatives (TBA)$_4$[γ-X$V_2W_{10}O_{38}$(μ-OH)(μ-OR)] (R = Me, Et, Pr) in moderate yields. **2^{Ge}·Me** (0.0335 g, 9.21 μmol, 67%), IR (KBr): 2961 m, 2931 m, 2873 m, 1484 m (ν(C−N)), 1383 w, 1152 w, 1107 w, 1048 w, 997 w, 961 s (ν(V═O)), 875 s, 849 s, 809 vs, 759 s, 690 m, 541 w, 463 w, 445 w, 395 w, 374 w, 347 w, 286 w, 253 s cm^{-1}. ^{1}H NMR (500 MHz, CD_3CN, r.t.) δ_H (ppm) 5.01 (s, 1H, O*H*), 4.43 (s, 3H, O*Me*), 3.16 (brs, 32H, NCH_2), 1.64 (brs, 32H, CH_2), 1.40 (q, ^2J = 6.9 Hz, 32H, CH_2), 0.99 (t, ^2J = 6.9 Hz, 48H, *Me*). ^{13}C{H} NMR (124.50 MHz, CD_3CN, r.t.) δ_C (ppm) 69.18 (O*Me*), 59.26 (NCH_2), 24.34 (CH_2), 20.32 (CH_2), 13.85 (*Me*). ^{51}V{H} NMR (130.23 MHz CD_3CN, r.t.) δ_V (ppm) −529.44. ^{183}W NMR (20.81 MHz, CD_3CN, r.t.) δ_W (ppm) −52.34 (2W), −63.65 (2W), −71.93 (1W), −98.58 (2W), −102.90 (1W), −109.64 (2W). CSI-MS (263 K, CH_3CN) *m*/*z* 3880.98 (*m*/*z* 3881.58 calcd for {(TBA)$_5$[$GeV_2W_{10}O_{38}$(OH)(OMe)]}$^+$). Anal. Calcd for $C_{65}W_{10}H_{148}V_2O_{40}GeN_4$: C, 21.46; H, 4.10; N, 1.54%. Found: C, 21.37; H, 4.05; N, 1.50%. **2^{Ge}·Et** (0.0419 g, 11.5 μmol, 83%), IR (KBr): 2961 m, 2933 m, 2873 m, 1483 m (ν(C−N)), 1382 w, 1153 w, 1106 w, 1042 w, 996 w, 962 s (ν(V═O)), 876 s, 809 vs, 760 s, 691 s, 542 w, 463 w, 443 w, 394 w, 374 w, 337 w, 278 m cm^{-1}. ^{1}H NMR (500 MHz, CD_3CN, r.t.) δ_H (ppm) 4.85 (s, 1H, O*H*), 4.51 (brs, 2H, OCH_2), 3.17 (brs, 32H, NCH_2), 1.80 (t, ^2J = 7.0 Hz, 3H, CH_3), 1.65 (brs, 32H, CH_2), 1.41 (q, ^2J = 7.5 Hz, 32H, CH_2), 0.99 (t, ^2J = 7.5 Hz, 48H, CH_3). ^{13}C{H} NMR (124.50 MHz, CD_3CN, r.t.) δ_C (ppm) 75.26 (OCH_2), 59.26 (NCH_2), 24.37 (CH_2), 20.34 (CH_2), 13.89 (CH_3 (OEt) & CH_3 (TBA)). ^{51}V{H} NMR (130.23 MHz, CD_3CN, r.t.) δ_V (ppm) −531.17. ^{183}W NMR (20.81 MHz, CD_3CN, r.t.) δ_W −53.23 (2W), −65.71 (2W), −75.08 (1W), −99.19 (2W), −101.00 (1W), −107.92 (2W). CSI-MS (263 K, CH_3CN) *m*/*z* 3895.91 (*m*/*z* 3895.59 calcd for {(TBA)$_5$[γ-$GeV_2W_{10}O_{38}$(OH)-(OEt)]}$^+$). Anal. Calcd for $C_{66}GeW_{10}H_{150}O_{40}N_4$: C, 21.70; H, 4.14; N, 1.53%. Found: C, 21.39; H, 3.92; N, 1.56%. **2^{Ge}·Pr** (0.0466 g, 12.7 μmol, 92%), IR (KBr): 3492 w (ν(O−H)), 2961 m, 2934 m, 2873 m (ν(C−H)), 1483 m, 1381 w, 1152 w, 1106 w, 1038 w, 995 m, 963 s (ν(V═O)), 876 s, 854 s, 809 vs, 760 s, 689 s, 540 w, 462 w, 445 w, 395 w, 374 w, 348 w, 256 m cm^{-1}. ^{1}H NMR (500 MHz, CD_3CN, r.t.) δ_H (ppm) 4.87 (s, 1H, O*H*), 4.36 (brs, 2H, CH_2), 3.17 (t, ^2J = 8.5 Hz, 32H, NCH_2), 2.42 (q, ^2J = 7.0 Hz, 2H, CH_2), 1.65 (quint, ^2J = 7.5 Hz, 32H, CH_2), 1.42 (q, ^2J = 7.5 Hz, 32H, CH_2), 1.01 (t, ^2J = 7.0 Hz, 3H, *Me*), 0.99 (t, ^2J = 7.5 Hz, 48H, *Me*). ^{13}C{H} NMR (124.5 MHz, CD_3CN, r.t.) δ_C (ppm) 81.59 (OCH_2, OPr), 59.29 (NCH_2, TBA), 24.39 (CH_2, TBA), 21.57 (CH_2, OPr), 20.35 (CH_2, TBA), 13.90 (CH_3, TBA), 10.32 (CH_3, OPr). ^{51}V{H} NMR (130.23 MHz, CD_3CN, r.t.) δ_V (ppm) −528.78. ^{183}W NMR (20.81 MHz, CD_3CN, r.t.) δ_W (ppm) −54.44 (2W), −66.62 (2W), −76.39 (1W), −100.26 (2W), −102.48 (1W), −109.06 (2W). CSI-MS (263 K, CH_3CN) *m*/*z* 3909.89 (*m*/*z* 3909.61 calcd for {(TBA)$_5$[γ-$GeV_2W_{10}O_{38}$(OH)-(OPr)]}$^+$). Anal. Calcd for $C_{67}GeW_{10}H_{152}V_2O_{40}N_4$: C, 21.95; H, 4.18; N, 1.53%. Found: C, 21.75; H, 4.03; N, 1.56%. **2^{Si}·Me** (0.0276 g, 7.68 μmol, 55%), IR (KBr): 3510 w (ν(O−H)), 2961 s, 2934 m, 2873 m, 1483 m, 1380 m, 1152 w, 1106 w, 1050 w, 1028 w, 1001 m, 992 w, 972 s, 964 vs, 918 vs, 902 vs, 871 vs, 788 vs, 783 vs, 703 s, 556 m, 409 m, 356 m, 332 m, 311 m, 289 m, 267 m, 252 s cm^{-1}. ^{1}H NMR (500 MHz, CD_3CN, r.t.) δ_H (ppm) 5.18 (s, 1H, O*H*), 4.44 (s, 3H, O*Me*), 3.16 (t, ^2J = 8.5 Hz, 32H, NCH_2), 1.65 (quint, ^2J = 7.0 Hz, 32H, CH_2), 1.41 (q, ^2J = 7.5 Hz, 32H, CH_2), 0.99 (t, ^2J = 7.5 Hz, 48H, *Me*). ^{13}C{H} NMR (124.50 MHz, CD_3CN, r.t.) δ_C (ppm) 69.20 (*Me*), 59.27 (NCH_2), 24.36 (CH_2), 20.33 (CH_2), 13.87 (*Me*). ^{29}Si{H} NMR (99.33 MHz, CD_3CN, r.t.) δ_{Si} −85.73. ^{51}V{H} NMR (130.23 MHz, CD_3CN, r.t.) δ_V (ppm) −548.05. ^{183}W NMR (20.81 MHz, CD_3CN, r.t.) δ_W (ppm) −80.29 (2W), −93.08 (1W), −93.97 (2W), −122.82 (1W), −124.07 (2W), −134.2 (2W). CSI-MS (263 K, CH_3CN) *m*/*z* 3836.25 (*m*/*z* 3836.63 calcd for {(TBA)$_5$[$SiV_2W_{10}O_{38}$(OH)-(OMe)]}$^+$). Anal. Calcd for $C_{65}W_{10}H_{148}V_2O_{40}SiN_4$: C, 21.72; H, 4.15; N, 1.56%. Found: C, 21.31; H, 4.12; N, 1.47%. **2^{Si}·Et** (0.0383 g, 10.6 μmol, 76%), IR (KBr): 3485 w (ν(O−H)), 2962 m, 2936 m, 2874 m (ν(C−H)), 1483 m (ν(C−N)), 1380 w, 992 w, 964 (ν(V═O)), 918 vs, 903 vs, 872 vs, 789 vs, 702 m, 555 m, 408 m, 389 m, 356 m, 330 m, 309 w, 303 w, 285 w, 256 m cm^{-1}. ^{1}H NMR (500 MHz, CD_3CN) δ_H (ppm) 5.05 (s, 1H, O*H*), 4.57 (q, ^2J = 7.0 Hz, OCH_2), 3.19 (t, ^2J = 8.0 Hz, NCH_2), 1.80 (t, ^2J = 7 Hz, 3H, CH_3), 1.67 (br, 32H, CH_2), 1.41 (q, ^2J = 7.5 Hz, 32H, CH_2), 0.99 (t, ^2J = 7.5 Hz, 48H, CH_3). ^{13}C{H} NMR (124.50 MHz, CD_3CN, r.t.) 75.48 (OCH_2, OEt), 59.26 (NCH_2, TBA), 24.37 (CH_2, TBA), 20.34 (CH_2, TBA), 13.88 (CH_3, TBA), 13.86 (CH_3, OEt). ^{29}Si{H} NMR (99.33 MHz, CD_3CN, r.t.) δ_{Si} (ppm) −85.73. ^{51}V{H} NMR (130.23 MHz, CD_3CN) δ_V (ppm) −549.09. CSI-MS (263 K, CH_3CN) *m*/*z* 3851.06 (*m*/*z* 3850.64 calcd for {(TBA)$_5$[$SiV_2W_{10}O_{38}$(OH)(OEt)]}$^+$). Anal. Calcd for $C_{66}W_{10}H_{150}V_2O_{40}SiN_4$: C, 21.97; H, 4.19; N, 1.55%. Found: C, 21.55; H, 4.16; 1.55%. **2^{Si}·Pr** (0.0314 g, 8.44 μmol, 61%), IR (KBr): 3489 (ν(O−H)), 2961 s, 2935 m, 2874 m (ν(C−H)), 1483 m (ν(C−N)), 1380 m, 992 m, 964 s (ν(V═O)), 918 s, 903 vs, 872 vs, 780 vs, 701 m, 557 m, 457 w, 407 m, 392 m, 356 m, 332 m, 310 w, 301 w, 286 w, 275 w, 270 w, 257 m, 252 m cm^{-1}. ^{1}H NMR (500 MHz, CD_3CN, r.t.) δ_H (ppm) 5.04 (s, 1H, O*H*), 4.40 (t, ^2J = 7.5 Hz, OCH_2), 3.17 (t, ^2J = 8.5 Hz, 32H, NCH_2), 2.38 (q, ^2J = 8 Hz, 2H, CH_2), 1.65 (quint, ^2J = 8.0 Hz, 32H, CH_2), 1.42 (q, ^2J = 7.5 Hz, 32H, CH_2), 1.04 (t, ^2J = 8.0 Hz, 3H, CH_3), 0.99 (t, ^2J = 7.5 Hz, 48H, CH_3). ^{13}C{H} NMR (124.50 MHz, CD_3CN, r.t.) δ_C (ppm) 81.75 (OCH_2), 59.26 (NCH_2, TBA), 24.37 (CH_2, TBA), 21.76 (CH_2), 20.34 (CH_2, TBA), 13.90 (CH_3, TBA), 10.35 (CH_3). ^{29}Si{H} NMR (99.33 MHz, CD_3CN, r.t.) δ_{Si} (ppm) −85.71. ^{51}V{H}NMR (130.23 MHz, CD_3CN, r.t.) δ_V (ppm) −546.55. ^{183}W NMR (20.81 MHz, CD_3CN, r.t.) δ_W (ppm) −81.59 (2W), −95.69 (3W), −121.49 (1W), −124.51 (2W), −132.31 (2W). CSI-MS (263 K, CH_3CN) *m*/*z* 3865.15 (*m*/*z* 3864.66 calcd for {(TBA)$_5$[$SiV_2W_{10}O_{38}$(OH)(OPr)]}$^+$). Anal. Calcd for $C_{67}W_{10}H_{152}V_2O_{40}SiN_4$: C, 22.22; H, 4.23; N, 1.55%. Found: C, 21.92; H, 4.18; N, 1.59%.

Spin−Orbit Variant of Individual Gauge for Localized Orbitals (SO-IGLO). To calculate NMR magnetic shielding constants, the spin−orbit variant of the individual gauge for localized orbitals (SO-IGLO) approach that is an extension of the conventional spin-free IGLO approach to the relativistic spin−orbit case was employed and implemented with the NTChem program package.[28] To satisfy the gauge invariance, the IGLO approach adopts individual gauge for localized orbitals,[33,34]

$$\phi_j = \exp\left(-\frac{i}{c}\mathbf{B}\cdot\mathbf{\Lambda}_j^{(\mathbf{B})}\right)\phi_j^{(0)} \tag{2}$$

with

$$\mathbf{\Lambda}_j^{(\mathrm{B})} = \frac{1}{2}(\mathbf{R}_j \times \mathbf{r}) \tag{3}$$

where c is the speed of light and $\mathbf{R}_j$ is a gauge origin for the jth localized orbital, which is usually defined by a centroid of charge of the localized orbital. To obtain the localized orbitals from the canonical orbitals, in this study, we used the Cholesky localization scheme proposed by Aquilante et al.[35] In the SO-IGLO approach, the magnetic shielding constant for a nucleus A in a closed-shell molecule is given by eq 1, where the first term is the diamagnetic shielding term, and the second term consists of paramagnetic, spin-dipolar, and Fermi contact terms in the presence of the spin−orbit interaction. While the first term of eq 1 is calculated by the expectation value with zeroth-order localized orbitals $\phi_i^{(0)}$, the second term is evaluated by the first-order orbitals $\phi_i^{(\mathbf{B})}$ with respect to magnetic fields. In the SO-IGLO approach, the zeroth-order canonical orbitals are directly obtained by the two-component spin−orbit density functional theory (SO−DFT) calculation. The first-order orbitals are expanded by a linear combination of occupied and virtual localized orbitals,

$$\phi_i^{(\mathbf{B})} = \sum_j^{\mathrm{occ}} \phi_j^{(0)}\mathbf{X}_{ji} + \sum_a^{\mathrm{vir}} \phi_a^{(0)}\mathbf{X}_{ai} \tag{4}$$

The first-order orbitals can usually be obtained by solving the coupled perturbed Kohn−Sham equation, but they are simply determined by the uncoupled DFT scheme in the pure DFT case. The occupied−occupied part of the coefficient matrix elements in eq 4 is given by

dx.doi.org/10.1021/ic5005209 | *Inorg. Chem.* 2014, 53, 3907−3918

$$\mathbf{X}_{ji} = -\frac{1}{2c}\left\langle \phi_j^{(0)} \middle| \mathbf{\Lambda}_j^{(\mathbf{B})} - \mathbf{\Lambda}_i^{(\mathbf{B})} \middle| \phi_i^{(0)} \right\rangle \quad (5)$$

The virtual−occupied part in eq 4 is given by

$$X_{ai} = \sum_k \sum_j \mathbf{Y}_{aj}\mathbf{D}_{kj}^{*}(\varepsilon_k - \varepsilon_a)^{-1}\mathbf{D}_{ki} \quad (6)$$

where ε_k and ε_a are the canonical orbital energies for occupied and virtual orbitals, respectively, and the matrix $\mathbf{D}$ is the transformation matrix from canonical to localized orbitals. The matrix $\mathbf{Y}$ is defined by

$$\mathbf{Y}_{aj} = \left\langle \phi_a^{(0)} \middle| \hat{h}_j^{(\mathbf{B})} \middle| \phi_j^{(0)} \right\rangle - \frac{1}{c}\sum_i \left\langle \phi_a^{(0)} \middle| \mathbf{\Lambda}_j^{(\mathbf{B})} - \mathbf{\Lambda}_i^{(\mathbf{B})} \middle| \phi_i^{(0)} \right\rangle \left\langle \phi_i^{(0)} \middle| \hat{f}^{(0)} \middle| \phi_j^{(0)} \right\rangle \quad (7)$$

where $\hat{f}^{(0)}$ is the zeroth-order KS operator. The magnetic operator $\hat{h}_j^{(\mathbf{B})}$ is composed of orbital and spin Zeeman operators.

Relativistic effects were considered by the Douglas−Kroll approximation.[36−38] The scalar relativistic effect was treated by the third-order DK approximation,[39] while the spin−orbit interaction was treated by the screened-nuclear SO (SNSO) approximation[40] with the first-order DK transformation. The finite-nucleus effect is also considered to obtain the zeroth-order KS orbitals. In addition, the picture-change effect on the magnetic interaction was considered by the simple relativistic correction to the magnetic perturbation within the free-particle (or first-order DK) approximation. The DK transformed one-electron magnetic operators could be derived from the following Hamiltonian including the magnetic interaction within the free-particle approximation,

$$H^{\mathrm{FP}} = A_p[c(\boldsymbol{\sigma}\cdot\boldsymbol{\pi})^2 K_p + cK_p(\boldsymbol{\sigma}\cdot\boldsymbol{\pi})^2 - 2c^2 K_p(\boldsymbol{\sigma}\cdot\boldsymbol{\pi})^2 K_p + V + K_p(\boldsymbol{\sigma}\cdot\boldsymbol{\pi})V(\boldsymbol{\sigma}\cdot\boldsymbol{\pi})K_p]A_p \quad (8)$$

with

$$(\boldsymbol{\sigma}\cdot\boldsymbol{\pi})^2 = \mathbf{p}^2 + \frac{1}{c}(\sigma\cdot\mathbf{p})(\boldsymbol{\sigma}\cdot\mathbf{A}) + \frac{1}{c}(\boldsymbol{\sigma}\cdot\mathbf{A})(\boldsymbol{\sigma}\cdot\mathbf{p}) + \frac{1}{c^2}\mathbf{A}^2 \quad (9)$$

Here, $\mathbf{p}$ is the canonical momentum and $\boldsymbol{\pi} = \mathbf{p} + (1/c)\mathbf{A}$ is the mechanical momentum with the vector potential $\mathbf{A}$. The kinetic operators A_p and R_p are defined by

$$A_p = \left(\frac{E_p + c^2}{2E_p}\right)^{1/2} \quad (10)$$

$$K_p = \frac{c}{E_p + c^2} \quad (11)$$

with

$$E_p = (p^2c^2 + c^4)^{1/2} \quad (12)$$

X-ray Crystallography. Diffraction measurements were made on Rigaku MicroMax-007 with Mo Kα radiation (λ = 0.71069 Å) at 153 K. Indexing was performed based on 12 oscillation images, each of which was exposed for 5 s at a crystal-to-detector distance of 45 mm. Readouts were based on a pixel size of 72.4 × 72.4 mm, and each data sweep was performed using ω scans from −110° to 70° at κ = 45° and ϕ = 0°, 90°. A total of 720 images were collected for each compound. Neutral scattering factors were obtained from a standard source,[41] data were corrected for Lorentz and polarization effects, and empirical absorption corrections were made with the HKL 2000 program for Linux.[42] Molecular structures were solved using the SHELX-97[43] program linked to Win-GX for Windows.[44]

CCDC 938548 (2^{Ge}·**Me**), 938549 (2^{Ge}·**Et**), 938550 (2^{Ge}·**Pr**), 938551 (2^{Si}·**Me**), 938552 (2^{Si}·**Et**), and 938553 (2^{Si}·**Pr**) contain the supplementary crystallographic data. These data can be obtained free of charge via www.ccdc.cam.ac.uk/conts/retrieving.html (or from the Cambridge Crystallographic Data Centre, 12, Union Road, Cambridge CB2 1EZ, UK; Fax: (+44) 1223-336-033; or deposit@ccdc.cam.ac.uk).

■ ASSOCIATED CONTENT

Supporting Information

Crystallographic data for 2^{X}·**R** (X = Ge, Si; R = Me, Et, Pr). Crystallography experimental details. DFT calculations for 2^{X}·**R**. Spectroscopic data for 2^{X}·**R**. Complete ref 19. This material is available free of charge via the Internet at http://pubs.acs.org.

■ AUTHOR INFORMATION

Corresponding Author

*Phone: +81-3-5841-7272. Fax: +81-3-5841-7220. E-mail: tmizuno@mail.ecc.u-tokyo.ac.jp.

Notes

The authors declare no competing financial interest.

■ ACKNOWLEDGMENTS

This work was supported by Grants-in-Aid for Scientific Research from the Ministry of Education, Culture, Science, Sports and Technology of Japan (MEXT) and the Funding Program for World-Leading Innovative R&D on Science and Technology (FIRST Program) of the Japan Society for the Promotion of Science (JSPS). Part of the calculation was performed at Research Center for Computational Science, Okazaki, Japan.

■ REFERENCES

(1) (a) Rehder, D. *Bioinorganic Vanadium Chemistry*; John Wiley & Sons, Ltd.: Chichester, West Sussex, 2008. (b) Rehder, D. *Coord. Chem. Rev.* **2008**, *252*, 2209−2223.

(2) Tatiersky, J.; Pacigová, S.; Sivák, M.; Schwendt, P. *J. Argent. Chem. Soc.* **2009**, *97*, 181−198 (and references cited therein).

(3) (a) Tracey, A. S. *Coord. Chem. Rev.* **2003**, *237*, 113−121. (b) Butler, A.; Eckert, H. *J. Am. Chem. Soc.* **1989**, *111*, 2802−2809.

(4) (a) Nakatsuji, H.; Inoue, T.; Nakao, T. *J. Phys. Chem.* **1992**, *96*, 7953−7958. (b) Nakatsuji, H.; Nakajima, T.; Hada, M.; Takashima, H.; Tanaka, S. *Chem. Phys. Lett.* **1995**, *247*, 418−424. (c) Melo, J.; Maldonado, A. F.; Aucar, G. A. *J. Chem. Phys.* **2012**, *137*, 214319. (d) Engesser, T. A.; Hrobárik, P.; Trapp, N.; Eiden, P.; Scherer, H.; Kaupp, M.; Krossing, I. *ChemPlusChem* **2012**, *77*, 643−651.

(5) (a) Maatta, E. A. *Inorg. Chem.* **1984**, *23*, 2560−2561. (b) Herberhold, M.; Schrepfermann, M.; Darkwa, J. *J. Organomet. Chem.* **1992**, *430*, 61−77. (c) Sayer, B. G.; Hao, N.; Dénès, G.; Bickley, D. G.; McGlinchey, M. J. *Inorg. Chim. Acta* **1981**, *48*, 53−55. (d) Minelli, M.; Yamanouchi, K.; Enemark, J. H.; Subramanian, P.; Kaul, B. B.; Spence, J. T. *Inorg. Chem.* **1984**, *23*, 2554−2556. (e) Ma, Y.; Demou, P.; Faller, J. W. *Inorg. Chem.* **1991**, *30*, 62−64. (f) Nakatsuji, H.; Hu, Z.−M.; Nakajima, T. *Chem. Phys. Lett.* **1997**, *275*, 429−436.

(6) The paramagnetic shielding constant term (σ_p) is defined as $-(\mathrm{const})\cdot(\Delta E_{av})^{-1}\cdot\langle r^{-3}\rangle\cdot c^2$, where ΔE_{av}, r, and c represent the average HOMO-LUMO energy gap, the expanse of the orbital of the observed nucleus toward the ligand, and the coefficient of the linear combination atomic orbital (LCAO), respectively Jameson, C. J.; Gutowsky, H. S. *J. Chem. Phys.* **1964**, *40*, 1714.

(7) (a) Gracia, J.; Poblet, J. M.; Autschbach, J.; Kazansky, L. P. *Eur. J. Inorg. Chem.* **2006**, 1139−1148. (b) Kazansky, L. P.; Yamase, T. *J. Phys. Chem. A* **2004**, *108*, 6437−6448. (c) Kazansky, L. P.; Chaquin, P.; Founier, M.; Hervé, G. *Polyhedron* **1998**, *17*, 4353−4364. (d) Inoue, M.; Yamase, T.; Kazansky, L. P. *Polyhedron* **2003**, *22*, 1183−1189. (e) Fedotov, M. A.; Samokhvalova, E. P.; Kazansky, L. P. *Polyhedron* **1996**, *15*, 3341−3351.

(8) (a) López, X.; Carbo, J. J.; Bo, C.; Poblet, J. M. *Chem. Soc. Rev.* **2012**, *41*, 7537−7571. (b) Vilà-Nadal, L.; Sarasa, J. P.; Rodíguez-Fortea, A.; Igual, J.; Kazansky, L. P.; Poblet, J. M. *Chem. Asian J.* **2010**, *5*, 97−104.

(9) Vankova, N.; Heine, T.; Kortz, U. *Eur. J. Inorg. Chem.* **2009**, 5102−5108.

(10) (a) Bagno, A.; Bonchio, M.; Autschbach, J. *Chem. –Eur J.* **2006**, *12*, 8460–8471. (b) Bagno, A.; Bonchio, M.; Sartorel, A.; Scorrano, G. *ChemPhysChem* **2003**, *4*, 517–519.
(11) (a) Thematic issues concerning polyoxometalates: Hill, C., Ed. *Chem. Rev.* **1998**, *98*, 1. (b) *Polyoxometalate Chemistry for Nano-Composite Design*; Yamase, T., Pope, M. T., Eds.; Kluwer: Dordrecht, The Netherlands, 2002. (c) Kozhevnikov, I. V. In *Catalysis by Polyoxometalates*; Wiley: Chichester, UK, 2002. (d) Pope, M. T. In *Comprehensive Coordination Chemistry II*; Wedd, A. G., McCleverty, J. A., Meyer, T. J., Eds.; Elsevier: New York, 2004; Vol. 4, p 635. (e) Hill, C. L. In *Comprehensive Coordination Chemistry II*; Wedd, A. G., McCleverty, J. A., Meyer, T. J., Eds.; Elsevier: New York, 2004; Vol. 4, p 679. (f) Neumann, R. In *Modern Oxidation Methods*; Bäckvall, J. E., Ed.; Wiley-VCH: Weinheim, 2004; p 223. (g) Yu, R.; Kuang, X.-F.; Wu, X.-Y.; Lu, C.-Z.; Donahue, J. P. *Coord. Chem. Rev.* **2009**, *253*, 2872–2890.
(12) (a) Bassil, B. S.; Kortz, U. *Dalton Trans.* **2011**, *40*, 9649–9661. (b) Miras, H. N.; Yan, J.; Long, D.–L.; Cronin, L. *Chem. Soc. Rev.* **2012**, *41*, 7403–7430. (c) Liu, H.; Gómez–García, C. J.; Peng, J.; Feng, Y.; Su, Z.; Sha, J.; Wang, L. *Inorg. Chem.* **2006**, *46*, 10041–10043.
(13) (a) Kuznetsov, A. E.; Geletti, Y. V.; Hill, C. L.; Morokuma, K.; Musaev, D. G. *Theor. Chem. Acc.* **2011**, *130*, 197–207. (b) Wang, Y.; Zheng, G.; Morokuma, K.; Geletii, Y. V.; Hill, C. L.; Musaev, D. G. *J. Phys. Chem. B* **2006**, *110*, 5230–5237. (c) Quiñonero, D. Q.; Wang, Y.; Morokuma, K.; Khavrutskii, L. A.; Botar, B.; Geletii, Y. V.; Hill, C. L.; Musaev, D. G. *J. Phys. Chem. B* **2006**, *110*, 170–173. (d) Musaev, D.; Morokuma, K.; Geletii, Y. V.; Hill, C. L. *Inorg. Chem.* **2004**, *43*, 7702–7708.
(14) (a) Mbomekallé, I.-M.; López, X.; Poblet, J. M.; Sécheresse, F.; Keita, B.; Nadjo, L. *Inorg. Chem.* **2010**, *49*, 7001–7006. (b) Poblet, J. M.; López, X.; Bo, C. *Chem. Soc. Rev.* **2003**, *32*, 297–308.
(15) (a) Besson, C.; Musaev, D. G.; Lahootun, V.; Cao, R.; Chamoreau, L.–M.; Villanneau, R.; Villain, F.; Thouvenot, R.; Geletii, Y. V.; Hill, C. L.; Proust, A. *Chem. –Eur. J.* **2009**, *15*, 10233–10243. (b) Knoth, W. H.; Harlow, R. L. *J. Am. Chem. Soc.* **1981**, *103*, 4265–4266.
(16) (a) Uehara, K.; Taketsugu, T.; Yonehara, K.; Mizuno, N. *Inorg. Chem.* **2013**, *52*, 1133–1140. (b) Uehara, K.; Mizuno, N. *J. Am. Chem. Soc.* **2011**, *133*, 1622–1625.
(17) The water-soluble tetramethylammonium (TMA) salt of divanadium(V)-substituted γ-Keggin-type silicodecatungstate, $(TMA)_4[\gamma\text{-}SiV_2W_{10}O_{38}(\mu\text{-}OH)(\mu\text{-}OMe)]$ was reported previously. (a) Nakagawa, Y.; Uehara, K.; Mizuno, N. *Inorg. Chem.* **2005**, *44*, 14–16. (b) Nakagawa, Y.; Uehara, K.; Mizuno, N. *Inorg. Chem.* **2005**, *44*, 9068–9075.
(18) Brese, N. E.; O'Keeffe, M. *Acta Crystallogr.* **1991**, *B47*, 192–197.
(19) Frisch, M. J. et al. *Gaussian09*, revision B.01; Gaussian, Inc.: Wallingford, CT, 2009.
(20) Tomasi, J.; Mennucci, B.; Cammi, R. *Chem. Rev.* **2005**, *105*, 2999–3094.
(21) Boese, A. D.; Martin, J. M. L. *J. Chem. Phys.* **2004**, *121*, 3405–3416.
(22) Weigend, F.; Ahlrichs, R. *Phys. Chem. Chem. Phys.* **2005**, *7*, 3297–3305.
(23) Molekel 5.4 (the molecular visualization program developed by the visualization group at the Swiss national supercomputing center, CSCS).
(24) For examples, see: (a) Weinstock, I. A.; Cowan, J. J.; Barbuzzi, E. M. G.; Zeng, H.; Hill, C. L. *J. Am. Chem. Soc.* **1999**, *121*, 4608–4617. (b) Pettersson, L.; Andersson, I.; Selling, A.; Grate, H. *Inorg. Chem.* **1994**, *33*, 982–993. (c) Nambu, J.; Ueda, T.; Guo, S.–X.; Boas, J. F.; Bond, A. M. *Dalton Trans* **2010**, *39*, 7364–7373. (d) Canny, J.; Thouvenot, R.; Tézé, A.; Hervé, G.; Leparulo-Loftus, M. *Inorg. Chem.* **1991**, *30*, 976–981. (e) Domaille, P. J. *J. Am. Chem. Soc.* **1984**, *106*, 7677–7687. (f) Mossoba, M. M.; O'Connor, C. J.; Pope, M. T.; Sinn, E.; Hervé, G.; Tézé, A. *J. Am. Chem. Soc.* **1980**, *102*, 6866–6867. (g) Domaille, P. J.; Watunya, G. *Inorg. Chem.* **1986**, *25*, 1239–1242. (h) Finke, R. G.; Rapko, B.; Saxton, R. J.; Domaille, P. J. *J. Am. Chem. Soc.* **1986**, *108*, 2947–2960. (i) Domaille, P. J.; Harlow, R. L. *J. Am. Chem. Soc.* **1986**, *108*, 2108–2109. (j) Mothé-Esteves, P.; Pereira, M. M.; Arichi, J.; Louis, B. *Cryst. Growth Des.* **2010**, *10*, 371–378. (k) Nomiya, K.; Nemoto, Y.; Hasegawa, T.; Matsuoka, S. *J. Mol. Catal., A* **2000**, *152*, 55–65.
(25) (a) Akitt, J. W. In *NMR and Chemistry, An Introduction to Modern NMR Spectroscopy*, 3rd ed.; Chapman & Hall: London, 1992. For example, (b) Belogolova, E. F.; Sidorkin, V. F. *J. Phys. Chem. A* **2013**, *117*, 5365–5376. (c) Kim, N.; Hsieh, C.-H.; Stebbins, J. F. *Chem. Mater.* **2006**, *18*, 3855–3859. (d) Chernyshev, K. A; Gostevskii, B. A.; Krivdin, L. B. *Russ. J. Org. Chem.* **2013**, *49*, 832–837. (e) Xu, Z.; Stebbins, J. F. *Solid State Nucl. Mag.* **1995**, *5*, 103–112.
(26) (a) Rodriguez, A.; Alemany, P.; Ziegler, T. *J. Phys. Chem.* **1999**, *103*, 8288–8294. (b) Schreckenbach, G.; Ziegler, T. *J. Phys. Chem.* **1995**, *99*, 606–611.
(27) Quantum chemistry group, Sapporo, Japan. The basis set obtained from website: http://setani.sci.hokudai.ac.jp/sapporo/Welcome.do; Noro, T.; Sekiya, M.; Koga, T. *Theor. Chem. Acc.* **2012**, *131*, 1124.
(28) NTChem 2013: http://labs.aics.riken.jp/nakajimat_top/ntchem_e.html.
(29) Grimme, S. *J. Comput. Chem.* **2006**, *27*, 1787–1799.
(30) The precise estimation of the chemical shifts is still one of the important research fields in quantum chemistry, since the reproducing the structure in solution with the proper basis sets and solvent model and taking into account the relativistic effect of the heavy metals are very difficult.[31]
(31) (a) Bühl, M. *Annu. Rep. NMR Spectrosc.* **2008**, *64*, 77–126. (b) Jochen, A. *Coord. Chem. Rev.* **2007**, *251*, 1796–1821.
(32) Nsouli, N. H.; Bassil, B. S.; Dickman, H.; Kortz, U.; Keita, B.; Nadjo, L. *Inorg. Chem.* **2006**, *45*, 3858–3860.
(33) Kutzelnigg, W. *Isr. J. Chem.* **1980**, *19*, 193–200.
(34) Schindler, M.; Kutzelnigg, W. *J. Chem. Phys.* **1982**, *76*, 1919–1933.
(35) Aquilante, F.; Pedersen, T. B.; de Merás, A. S.; Koch, H. *J. Chem. Phys.* **2006**, *125*, 174101.
(36) Douglas, M.; Kroll, N. M. *Ann. Phys.* **1974**, *82*, 89–155.
(37) Hess, B. A. *Phys. Rev. A* **1986**, *33*, 3742–3748.
(38) Nakajima, T.; Hirao, K. *Chem. Rev.* **2012**, *112*, 385–402.
(39) Nakajima, T.; Hirao, K. *J. Chem. Phys.* **2000**, *113*, 7786–7789.
(40) Boettger, J. C. *Phys. Rev. B* **2000**, *62*, 7809–7815.
(41) *International Tables for X-ray Crystallography*; Kynoch Press: Birmingham, U.K., 1975; Vol. 4.
(42) Otwinowski, Z.; Minor, W. *Processing of X-ray Diffraction Data Collected in Oscillation Mode, Methods in Enzymology, Macromolecular Crystallography, Part A*; Carter, C. W., Jr., Sweet, R. M., Eds.; Academic Press: New York, 1997; Vol. *276*, p 307.
(43) Sheldrick, G. M. *SHELX-97, Programs for Crystal Structure Analysis*, release 97-2; University of Göttingen: Göttingen, Germany, 1997.
(44) Farrugia, L. J. *J. Appl. Crystallogr.* **1999**, *32*, 837–838.